Graz University of Technology

Institute of Biomechanics
Center of Biomedical Engineering
Kronesgasse 5-I
8010 Graz, Austria

Master Thesis

Determination of the mechanical strength of healthy and dissected human thoracic aortas subjected to different loading modes

to achieve the degree of
Master of Science

Author: Franz Seiringer, BSc.
Supervisor: Gerhard Sommer, PhD

Head of Institute: Professor Gerhard A. Holzapfel, PhD

March 18, 2015

Contents

List of Figures

List of Tables

Abstract

Aortic dissection is an acute life-threatening disease of the aorta which affects about 10 of 100.000 people per year. The underlying mechanics remain unclear, hence the research of aortic dissection is an important area of biomechanics.

The scope of this thesis lies in the investigation of the mechanical strength of healthy and diseased human thoracic aortas under a combination of uniaxial tension- and triaxial shear tests which are very rarely explored. The present diploma thesis is part of a major project (development of a 3D failure criterion for the healthy and dissected human aortic media) of the Institute of Biomechanics, Graz University of Technology. The project takes place within the framework of cooperation with the Department of Cardiac Surgery, Graz and the New York University School of Medicine.

The aortic tissue specimens have been investigated with the aid of an uniaxial- and triaxial testing device with respect to their orthotropic character. The ultimate strength values during uniaxial tension tests in the axial, circumferential and radial directions and additional in-plane (axial-circumferential plane) and out-of-plane shear tests in different orientations of layer-separated tissue were gathered and analyzed using $MATLAB^{®}$. To our knowledge there are no data available with the combination of performed tests. Moreover, performing out-of-plane shear tests on thoracic aortic tissue is novel.

A total of 13 human thoracic aortic tissues were investigated from which it is evident that the aortic media increases its strength under tension loading as follows: radial (normal direction) < axial (cross-fiber direction) < circumferential (fiber direction). Furthermore, this thesis shows new consolidated findings that the media is much stronger under out-of-plane shear loading than under in-plane shear loading. The results show clearly interspecimen differences because of the anamnesis of the donors, such as age, diseases, and other risk factors. Furthermore, anisotropic and nonlinear tissue properties are apparent from the experimental data.

Kurzfassung

Aortendissektion ist eine akute lebensbedrohliche Erkrankung der thorakalen Aorta, die etwa 10 von 100.000 Menschen pro Jahr betrifft. Die zugrunde liegende Mechanik ist unbekannt, weshalb die Erforschung der Aortendissektion einen wichtigen Bereich in der Biomechanik darstellt.

Der Rahmen dieser Arbeit umfasst die Untersuchung der mechanischen Festigkeit von gesunden und dissektierten menschlichen Brust-Aorten mittels einer Kombination aus einachsigen Zug- und triaxialen Scherversuchen. Die vorliegende Masterarbeit ist Teil eines großen Projekts (Entwicklung eines 3D-Fehlerkriteriums für die gesunde und dissektierte Media der menschlichen Aorta) des Instituts für Biomechanik der TU Graz. Das Projekt findet im Rahmen einer Kooperation mit der Klinik für Herzchirurgie, Medizinische Universität Graz und der New York University School of Medicine statt.

Die Gewebeproben der Aorten wurden mit Hilfe einer einachsigen und dreiachsigen Testmaschine unter Berücksichtigung ihrer orthotropen Eigenschaften untersucht. Die maximalen Festigkeitswerte während einachsiger Zugversuche in axialer-, umfangs- und radialer Richtung sowie von in-plane (Axial-Umfangsrichtungsebene) und out-of-plane Schertests in unterschiedlichen Richtungen wurden durchgeführt und mit *MATLAB*® analysiert. Unseres Wissens gibt es bis heute keine vorhanden Daten von der Kombination der angewandten Tests und der Durchführung von out-of-plane Scherversuchen an thorakalem Aortengewebe.

Insgesamt wurden 13 menschliche thorakale Aortengewebe untersucht, wobei offensichtlich ist, dass die Media der Aorta ihre Steifheit unter Zugbelastung wie folgt erhöht: Radialrichtung (Normalrichtung) < Axialrichtung (Querfaserrichtung) < Umfangsrichtung (Faserrichtung). Außerdem zeigt diese Arbeit neue Erkenntnisse, dass die Media viel stärker unter out-of-plane Scherbelastung als unter in-plane Scherbelastungen ist. Die Ergebnisse zeigen deutlich Unterschiede zwischen den Proben aufgrund der Anamnesen des jeweiligen Spenders, wie zum Beispiel, Alter, Krankheiten und anderen Risikofaktoren. Desweiteren sind anisotrope und nichtlineare Gewebeeigenschaften aus den experimentellen Daten ersichtlich.

Acknowledgment

This Master Thesis has been carried out at the Institute of Biomechanics, Graz University of Technologie in 2014/2015. I would like to express my gratitude to all people who supported me. First of all, I would like to give special thanks to my supervisor Dr. Gerhard Sommer for his great guidance during the whole master thesis, and his contribution of valuable knowledge, experience and advice.

I also would like to thank the head of the Institute of Biomechanics, Graz University of Technology, Prof. Dr. Gerhard Holzapfel, for the opportunity of writing my Master Thesis and for providing the laboratory facilities. Being a part of this office was very nice.
Further, I want would like to thank Dr. med. Peter J. Oberwalder from the Department of Cardiac Surgery, Medical University of Graz, for the great cooperation and providing a variety of human samples.

A great benefit was the support of Selda Sheriova, MSc, who gave me tips in all questions, and especially the help of my cousin Stefan Seiringer, who supported me in the construction of a punching tool for the tissue preparation.

Last but not least, I want to thank my parents and especially my girlfriend Daniela who always supported and motivated me throughout my years at university.

1 Introduction

In order to provide a background for this thesis, this chapter describes the physiology and the mechanics of the aorta as well as age-related changes of the artery. Further, it provides a brief overview of aortic dissection and aneurysm.

1.1 Motivation

Acute thoracic aortic dissection is a life-threatening disease of the main artery which is characterized by a disorder of the aortic wall, mostly by an initial tear of the inner vessel wall with subsequent hemorrhage between the layers. In general it causes strong, sudden pain and is immediately life-threatening because it can lead to aortic rupture and to acute vascular disorders of various organ systems. Despite prompt diagnosis and quickly initiated operative restructuring, the acute lethality is still at about 30% (Sodeck et al., 2008). Hence, for better understanding of this cause of death, it is clear that fundamental research of the underlying aspects should be made. For a better understanding the mechanical failure behavior of human thoracic aortic tissues has to be determined with the aid of uniaxial tension- and triaxial shear tests. Also biaxial tension tests are going to be conducted. We are still in process to develop the setup for this test.

The main aim of this study is the experimental exploration of important tissue parameters which are used for the computational modeling of the propagation of aortic dissection. Within a project of the Institute of Biomechanics, Graz University of Technology, attempts are made to derive a 3D failure criterion for the healthy and dissected human aortic media using the Tsai-Wu criterion. To employ the Tsai-Wu criterion, strength values at different loading modes through various mechanical tests are needed. In this thesis, data of human aortic medias were determined by performing a variety of uniaxial tension and triaxial shear tests. It is also necessary to obtain data of biaxial tension tests to include the influences of stress coupling between circumferential and axial direction in the Tsai-Wu criterion. The development of this test is still in progress. The ultimate goal of this project will be the development of a mathematical model and finite element simulations of the failure behavior of healthy and dissected aortic thoracic tissues, e.g. for developing better aortic grafts.

This Master Thesis is part of a research project by the Institute of Biomechanics, Graz University of Technology in cooperation with the Department of Cardiac Surgery, Medical University Graz, and the School of Medicine, New York University, that is focused on the determination of the mechanical strength of healthy and dissected human thoracic aortic tissues which are not explored so far. Additionally, to our knowledge there is no study that

has ever dealt with a combination of tension- and triaxial shear tests on human arterial thoracic tissue.

1.2 Physiology of the Aorta

A brief overview of the structure and the composites of arterial walls is provided in this chapter. Arteries can be roughly divided into 2 groups: muscular and elastic. Muscular arteries have small diameters and are located at the periphery, i.e. brachial, femoral and cerebral arteries. The latter are relatively large vessels that are located close to the heart, i.e. the ascending, thoracic and abdominal aorta as well as the carotid and iliac arteries. Their elastic properties make a significantly contribute to the smoothing of pulsating blood pressure waves (systolic–diastolic). The pulsatile load is balanced by the elastic arteries in the form of a circumferential elastic strain. The translation from muscular type to elastic type exhibits morphological structures of both types. In general, blood vessels consist of three concentric layers, the *tunica intima* (intima), the *tunica media* (media), and the *tunica adventitia* (adventitia). A representative schematic is shown in Fig. 1.1 (Holzapfel et al., 2000a; Sommer, 2010).

The intima consists of a single layer of endothelial cells and lines the inner surface of an artery, attached to a thin collagenous basal lamina. It fulfills the function of a semipermeable membrane which transmits chemical signals and delivers nutrients from the bloodstream in order to supply the vessel wall. The intima does not make a substantial contribution to the mechanical properties of the arterial wall in healthy young individuals. It is separated from the media by a sheet of elastin, the so called internal elastica lamina. It is important to note, that the intima thickens and stiffens with increasing age, which causes changes in the mechanical response. One of the reasons therefore may be atherosclerosis which leads to changes of the intimal components. Depositions of various constituents such as calcium, collagen fibers, fatty substances, cellular waste products and fibrin. These pathological changes result in atherosclerotic plaques. A further explanation about atherosclerotic plaque formation is in Section 1.2.1. (Holzapfel et al., 2000a; Sommer, 2010). .

The media is the middle layer of the artery, embedded between the internal elastic lamina and the external elastic lamina (the border to the adventitia) and it is a thick layer composed of a complex 3-dimensional network of smooth muscle cells that are embedded in an extracellular matrix (ECM) of elastin and collagen fibers and proteoglycans. Elastin provides the elasticity of the aortic wall. The mechanical properties of the media are an essential part in a healthy artery. A variety of fenestrated elastic laminae divides the media into concentrically fiber-reinforced medial layers. There are interconnections between the elastic fibers, collagen fibers, smooth muscle cells and the elastic laminae. Concerning to the orientation of the fibers in the media, the helix has a small pitch, so that one can say they are mostly orientated in the circumferential direction. Investigation of the mechanical properties of arterial walls was the main focus of this thesis, whereby mostly the media was examined (Holzapfel et al., 2000a; Sommer, 2010).

Finally, the adventitia consists of a dense network of collagen fibers that form a fibrous tissue. There are also cells situated such as fibroblasts and fibrocytes that produce collagen and ground matrix. Furthermore, there are nerves and vasa vasorum supplying the vessel with blood. The adventitia is the outermost layer of the vessel wall and is surrounded by loose connective tissue. The undulated collagen fibers are arranged in helical structures. At high levels of pressure the protective mechanism of the adventitia comes to the fore. The fibers of the adventitia extend gradually and get stiffer, preventing rupture of the artery in case of an significant increase in pressure (Holzapfel et al., 2000a; Sommer, 2010).
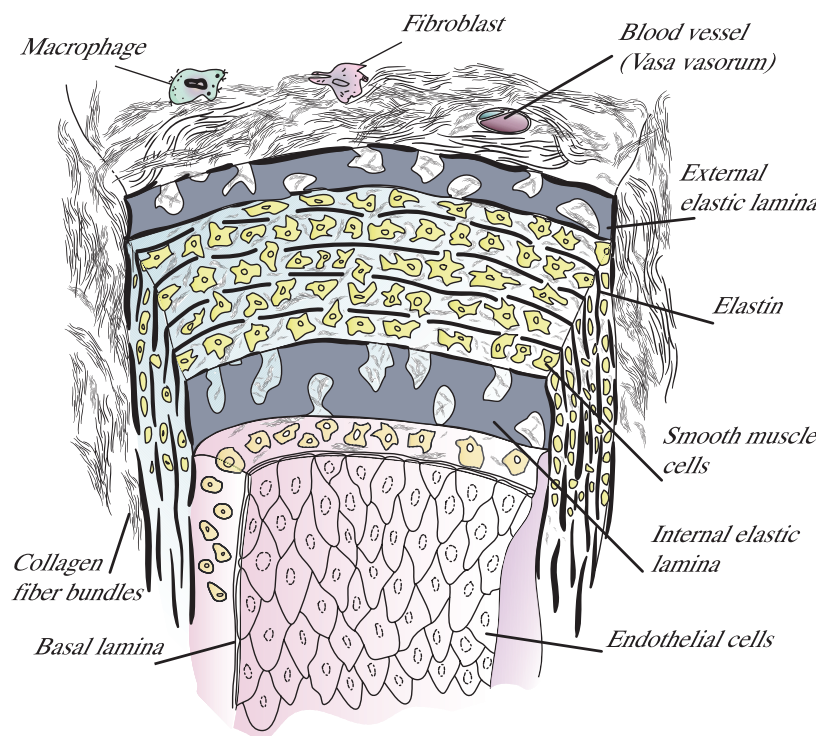
Figure 1.1: Structure of elastic arteries featuring the three concentric layers, *tunica intima*, *tunica media*, and *tunica adventitia* and their major components. Adapted from Rhodin (1979).

There are 28 different types of collagen proteins detected in the human body up to now. They can be associated with their structural properties. Collagen has great tension strength and is responsible of the nonlinear properties of most soft biological tissues (Holzapfel et al., 2000a). The major types in human vasculature are the fibrillar collagen type I and type III (Wu et al., 2013). Almost all collagen types in the intima and media of arterial walls are synthesized by smooth muscle cells and in the adventitia by fibroblasts. The newly formed collagen fibrils are connected by proteoglycans and form into cable-like helical fibers with cross links. Due to this, collagen is he main load carrying element of

arterial walls(Alberts et al., 2007). The sheetforming, nonfibrillar and basement membrane associated collagen type IV is located in the surrounding of smooth muscle and endothelial cells. Those collagen type IV molecules are arranged in a sheet network (Wu et al., 2013). Collagen fibers are connected to smooth muscle cells by the attachment protein fibronectin, which has interconnections to myosin and actin by integrin dimers (Alberts et al., 2007).

Elastin is the main component of elastic fibers, and is thus a decisive factor for the elastic behavior of artery walls.

1.2.1 Atherosclerosis

Atherosclerosis is a collective term for degenerative changes in the artery wall. It affects arterial blood vessels and is likely to lead to relevant diseases like coronary artery disease, peripheral arterial occlusive disease and cerebrovascular disorders. Due to those cases, it is important to reduce the risk factors for developing atherosclerosis. The pathogenesis of atherosclerosis is an interesting field of science because the exact way for developing atherosclerosis is still not completely understood. Atherosclerosis characterizes a chronic disease of the arterial wall and is the leading cause of death and reduced lifespan in the world. It is a focally localized disease of the intima associated with wall changes, sclerosis, loss of elasticity, plaque formation and lumen constriction of the vessel. Rupture of an unstable plaque can cause thrombosis of the affected vascular segment. As can be seen in the following description of the development of an atherosclerotic plaque, the mechanics and the structure of the wall changes significantly (Lusis, 2000; Polster et al., 2008).

Atherosclerosis is a progressive disease due to accumulation of lipids and fibrous elements in the large arteries. It is indicated by inflammatory processes in the endothelial cells of the vessel wall. The lumen of the vessel decreases gradually, sometimes up to blocking the blood flow. The healthy endothelium produces substances like nitrogen monoxide (NO) which prevents the accumulation of blood cells such as thrombocytes. This endothelial function is reduced by certain cardiovascular risk factors, such as an increased concentration of low density lipoproteins (LDL) in the blood. Thus, the bioavailability of nitrogen monoxide is reduced and cholesterol-containing LDLs are going to transmigrate across the endothelial layer into the intima. Being in the vessel LDLs react by attracting monocytes (white blood cells, part of leukocytes). They differentiate into macrophages after penetrating from the blood stream into the arterial wall. The macrophages accumulate lipids and cholesterol esters which become foam cells. High density lipoprotein (HDL) is a molecule which is responsible for the removal of cholesterol of the tissue. The higher the HDL concentration, the lower the risk of an atherosclerotic disease. After some time, the foam cells die and give their lipid substances to the necrotic core of the lesion. After that, some fatty steaks bind smooth muscle cells which come from the media. With the proliferation of smooth muscle cells, atherosclerotic plaques develop and increase in size. The lesion grows by accumulating mononuclear cells from the blood stream. The inflammation of the artery leads to degradation of collagen and, thus, triggers the formation of atherosclerotic plaques. In the final stage, the media is affected, which leads to loss of its elastic prop-

erties (Polster et al., 2008; Lusis, 2000). A schematic illustration of the progression of atherosclerosis is given in Fig. 1.2. An atherosclerotic plaque can either be stable, only affecting the blood flow, or unstable, being a potential source of risk for rupture and a source for thrombogenic contents. It is not the size of the plaque but rather the composition of the plaque that increases the risk (Sommer, 2010).
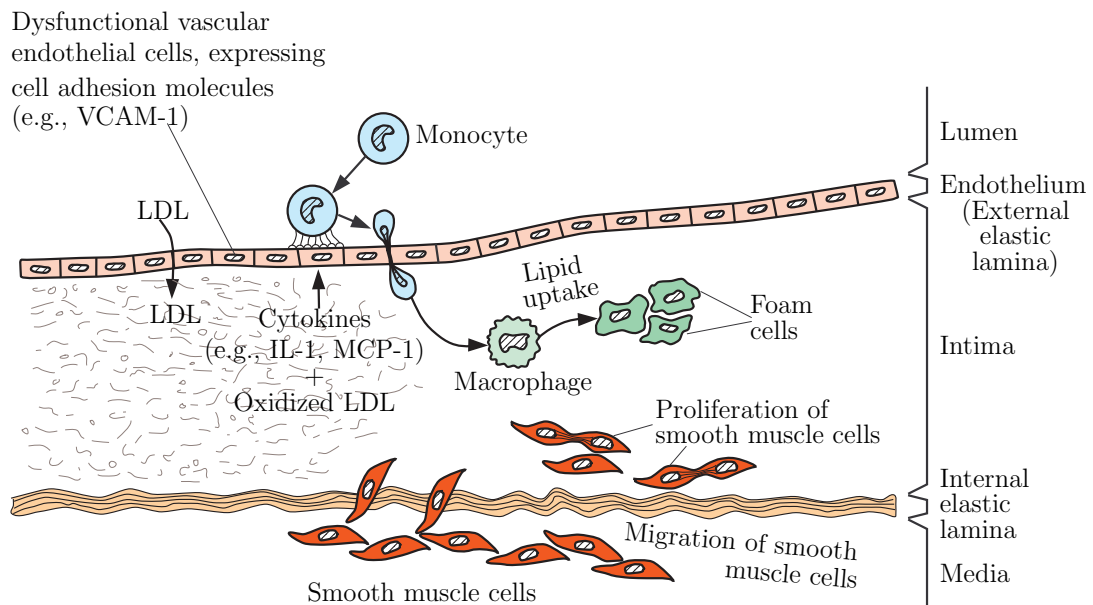
Figure 1.2: Progression of atherosclerosis. Starting from the initial state, where transmigration of the LDL through the endothelium into the intima takes place (left side) up to the beginning of the formation of atherosclerotic plaques (right side). Illustration adapted from Hulthe and Fagerberg (2002).

Some risk factors for arteriosclerosis are age, male gender and genetic predisposition. Smoking, adiposity, arterial hypertension and hypercholesterolemia are factors that increase the probability of atherosclerosis. Furthermore, factors like little exercise, overweight, high LDL, low HDL, diabetes mellitus and hyperthyroidism can have a negative impact. Treatments are based on a healthy way of life (i.e. sports, low-fat consumption). There is no medication that can dissolve the plaques. Diabetes, hypertension and hypercholesterolemia medication can be used for therapy. In serious cases, surgery with a catheter, stent, or balloon may be necessary (Polster et al., 2008).

1.3 Arterial Mechanics

1.3.1 Material Symmetry

The histology of arterial walls shows that the structural components are aligned in a specific direction. Smooth muscle cells in the media are arranged in the circumferential direction; however, type I collagen as a component of the adventitia is aligned axially. Furthermore, elastin of elastic arteries is arranged in thin concentric sheets (Humphrey, 2002). The histological structure of an artery is in the radial-axial plane and the radial-circumferential plane symmetrical, this means that a cylindrical orthotropy exists in the aorta. The term cylindrical orthotropy means the presence of three orthogonally arranged planes of symmetry in a material. This was proven by Patel and Fry (1969) based on canine aorta and carotid artery experiments. Their data demonstrated that the shear deformation in artery wall under physiological stress is an order of magnitude smaller than the shear deformations in the axial and circumferential directions. This suggests that the global response is cylindrically orthotropic (Patel and Fry, 1969).
In general, it should be noted that arterial walls exhibit an (locally) anisotropic behavior, implying distinct properties in all directions with respect to the load-free configuration. This is reflected with a different mechanical behavior in the axial and circumferential directions. The difference of the mechanical behavior within the different layers is attributed to the orientation of the load carrying wavy collagen fibrils (Holzapfel et al., 2000b).

1.3.2 Heterogeneity

Considering the cross section of an elastic artery, see Fig. 1.1, the three layers intima, media, and adventitia show that the artery is heterogeneous in the radial direction. However, the individual layers are homogeneous in the axial and circumferential direction. This is explained by the equability of the composition within each layer (Sommer, 2010). In contrast to the other layers, the intima is very thin, therefore the contribution to the load-bearing capacity of the aorta is not very high (Burton, 1954). The largest part of the load is taken by the media and adventitia. The first mechanical data on the response of the media and the adventitia were delivered by Vito and Demiray (1982). They carried out uniaxial tests in circumferential and axial direction on strips of the media and adventitia of a canine aorta. They showed that the media behaves less stiff than the adventitia, assuming that both were practically isotropic. At a later time they found out that the media is cylindrically orthotropic (Demiray and Vito, 1991).

1.3.3 Residual Stress

It is known that excised, unloaded arteries which are free of externally applied loads are not free of stress. They are subjected to circumferential and axial residual stresses. If an arterial ring is cut along its axial direction, it opens up to a specific angle. The residual stresses can be calculated from the opening angle. The opening angle is relatively independent of the

temperature of the solution in a range from -25°C to 40°C (Badrek-Amoudi et al., 1996; Holzapfel et al., 2000a). Residual stress involves a viscoelastic aspect, because the opening angle increases within 15 to 30 minutes after getting cut (Han and Fung, 1991).

Many authors have shown that residual stresses have a strong impact on the *in vivo* stress distribution in arteries. It should be mentioned in this context that residual stresses are dependent on the location and the layer (Holzapfel et al., 2007).

1.3.4 Incompressibility

Incompressibility is commonly assumed for arterial walls. This assumption is used to calculate and interpret the results of this thesis properly. With the help of incompressible behavior we are able to determine the mechanical behavior of a three-dimensional specimen by three-dimensional tests (Holzapfel et al., 2000a). Many investigations on the arterial wall have shown that arterial tissue behaves as a hyperelastic incompressible material. This means that the artery preserves its volume under load and shows an approximately isochoric behavior, which was shown by Lawton (1954). This assumption is underscored by the factor that soft tissues consist largely of water (about 70% to 80%). An artery consists of different constitutents such as solid parts like elastin, collagen and smooth muscle, and a fluid part which is mostly water.

The Poisson ratio is the fraction of expansion divided by the fraction of compression, in other words the ratio of relative thickness change to relative length change. For linear elasticity, the incompressibility implies that the bulk modulus is much greater than the shear modulus (Humphrey, 2002). For example, rubber has a Poisson's ratio close to 1/2, a bulk modulus of the order of GPa, and shear modulus of the order of MPa (Greaves et al., 2011). Concerning the atherosclerotic arteries, the assumption of incompressibility has to be revoked. The area of an atherosclerotic plaque has a composition that is not the same as in healthy arterial tissue. It could contain a high lipid content that behaves compressible (Sommer, 2010).

1.3.5 Stress-strain response

Considering the biomechanical perspective, the healthy arterial wall represents a deformable composite structure that shows under high pressures a nonlinear stress-strain response associated with a stiffening effect (Holzapfel et al., 2000a). This nonlinear stiffening effect results from the recruitment of the wavy collagen fibers, which are known as the main load-carrying element in the arterial wall.

At low blood pressure the stress is linear dependent on strain and the elastic tissue components dominate the mechanical response. If the strain increases to a higher blood pressure, the load is progressively transferred towards the collagen fibers. As a result they become aligned and more straightened, which leads to the already mentioned stiffening effect (nonlinear) and anisotropic mechanical behavior (Nichols and O'Rourke, 1998).

The stress-strain response of arterial walls can be divided into two domains: the elastic

and the inelastic. In the case of the elastic domain, typical uniaxial extension experiments have shown that cyclic loading and unloading is associated with stress softening effects. This needs a "pre-conditioning" of the tissue resulting in a nearly repeatable cyclic behavior Fung et al. (1979). In the "preconditioned" state, the tissue shows a nearly elastic behavior, which is referred in the literature as "pseudo-elastic" by Fung et al. (1979). This means that the tissue is elastic but has different loading and unloading cycles. Note that distal arteries of the muscular type exhibit viscoelastic behavior, while proximal arteries exhibit (perfectly) elastic behavior. If loading goes beyond the (visco)elastic domain, the inelastic domain is reached. The tissue undergoes inelastic deformation (elastoplastic and/or damage mechanism) causing irreversible changes in the mechanical behavior. This type of deformation is far beyond the range of physiological loading. However, it may occur during surgical treatments such as angioplasty (Holzapfel et al., 2000a).

1.4 Aortic Dissection

1.4.1 General facts

Aneurysms and aortic dissections are among the most common diseases of the thoracic aorta. In almost all cases a surgical intervention is necessary. An aneurysm is a permanent and irreversible dilatation of an arterial blood vessel. Aortic aneurysms are not easy to diagnose because of their protective, deep, intrathoracal and retroperitoneal location. Furthermore, the majority does not show any symptoms. The first manifestation of aneurysms is often a sudden rupture as a consequence of acute aortic wall dissection. In general one can say if the diameter reaches more than twice of the normal size the dilatation is called aneurysm (Oberwalder, 2001b).

   In this work, the main focus was placed on the aortic dissection. Aortic dissection is an acute life-threatening disease of the thoracic aorta and is said to be the most severe event concerning the aorta. In contrast to aortic aneurysm in which all wall layers are going to enlarge, the aortic dissection leads to a splitting of the wall layers (Polster et al., 2008). It usually occurs along the right lateral wall of the ascending aorta, where the hydraulic shear forces are high. Another common location is the descending aorta, immediately after the ligamentum arteriosum (Dietel et al., 2005). Aortic dissection occurs when an initial tear through the aortic intima takes place and directly propagates in the radial direction through the medial layer. After that the tear propagates axially, whereby the dissection can proceed further in antegrade (forward propagation), which is more common than retrograde (backwards propagation). This allows the blood flow to enter the aortic wall, whereby a secondary channel, a so called false lumen, is created. Intima and inner media limit the original real lumen and adventitia and external media form the false one. The false lumen continues the propagation in a spiraled or straight manner. The high pressure in the false lumen can lead within minutes to rupture of the adventitia (outer layer) causing the patient to bleed to death. If the blood flow of the false lumen enters back into the true lumen via a new intimal tear, it is known as an "re-entry". The propagation of the dissection in the

axial direction, either leads to detachment of the media from the adventitia, or the cleavage of the media itself. However, in the majority, medial splitting leads to weakness in the wall of the false lumen which in turn leads to a higher probability of developing dilatation and rupture (Criado, 2011; Oberwalder, 2001a).

The propagation is triggered by pulsatile blood which enters through the tear. Shear forces may trigger additional tears in the media, which may lead further to aortic wall rupture. Systolic pressure and the related increased diameter within the false lumen decreases the blood flow in the true lumen and may lead to malperfusion or ischemia of end-organs or limbs. Aortic intramural hematoma (IMH), which is known as a prestige of dissection, developed inside the medial wall layer from a ruptured vasa vasorum. This can also be a reason for classic aortic dissection, which is generally located in the descending aorta. Approximately 20% of intramural hematoma develops into full aortic dissections. The extension of the dissection depends on the blood pressure as the driving force and the resistance of the media. In the worst case it involves the entire length of the aorta up to the iliac arteries (Akin et al., 2010; Criado, 2011).

1.4.2 Classification

Aortic dissection can occur in any location of the aorta. According to different authors there are two major classifications to specify the aortic dissection. The older DeBakey classification and the newer Stanford classification, see Fig. 1.3. There is also a division in "proximal" and "distal" dissection (Criado, 2011; Ayala and Chen, 2012; Oberwalder, 2001a).

DeBakey classification

There are three different types of DeBakey classification with respect to localization of the intimal tear in the aortic wall (entry) and the length of the axial expansion of the false lumen.

- Type *I*: The primary tear is located in the ascending aorta, followed by an expansion of the dissected false lumen in the aortic arch or further in the entire aorta.

- Type *II*: Only the ascending aorta is affected by the dissection and the double lumen appears only in the ascending aorta.

- Type *III*: Only effects the descending aorta and is further divided into Type *IIIa* and Type *IIIb*.

    - Type *IIIa*: The dissection is only located in the descending aorta, proximal to the diaphragm.

    - Type *IIIb*: The dissection reaches up to the abdominal aorta, below the diaphragm.

Stanford classification

In this case, the axial expansion of the dissection is not considered.

- Type A: Summarizes DeBakey Type *I* and Type *II*. Includes any dissection that effects the ascending aorta (proximal dissection).

- Type B: Is equal to DeBakey Type *III*. Only the descending aorta is affected, with independent expansion of the false lumen in distal direction (distal dissection).

Another subdivision of aortic dissection can be done with the terms "proximal" and "distal". Proximal is concerning dissections proximal to the root of the left subclavian artery, regardless of the region distal to this anatomical point. In contrast, the term "distal" refers to the region of the thoracic aorta distal to the left subclavian artery, regardless of the aorta proximal to this point. The duration of symptoms leads to the classification at "acute", "sub-acute" and "chronic" of the disease. If the diagnosis is made within two weeks from symptom onset, the dissection is considered as acute. It is called as subacute case if 15 – 28 days elapse between the onset of symptoms and diagnosis. If the diagnosis lasts more than 28 days, it is defined as chronic (Ayala and Chen, 2012).

1.4.3 Incidence & Mortality

The incidence of aortic dissection is indicated in the literature with 10 cases per 100.000 people per year, whereas the frequency of an aortic aneurysm is 6 per 100.000 people per year. It mostly occurs in older persons (>fifty years). In patients with Marfan syndrome it usually occurs earlier. In fact, in less then 10% of all cases, people affected are younger than 40 years. In 68% of cases men are affected, whereas women only in 32%. These factors can either be traumatic or due to any disease, which weakens or degenerates the aortic media (Oberwalder, 2001a).

In the case of Stanford acute type A dissection, the mortality rate is about 1% per hour initially. According to the International Registry of Acute Aortic Dissection (IRAD (2014)) the mortality rate is 33% within the first 24 hours of untreated patients, 50% within the first 48 hours and nearly 80% up to the end of the second week, whereby the mortality rate decreases after two weeks for surviving patients. The survival rate in case of type B dissection is given as 65% after one month (Criado, 2011; Oberwalder, 2001a).
As described in a study by Hagan et al. (2000) the mortality of those patients treated surgically was 26%, whereas 58% of the patients died when surgery was not performed. In the case of type B dissection, 11% of the people who received medical treatment did not survive. 20% of the patients treated surgically which led to a mortality of 31%. If a surgical intervention is done the prognosis of patients increases.
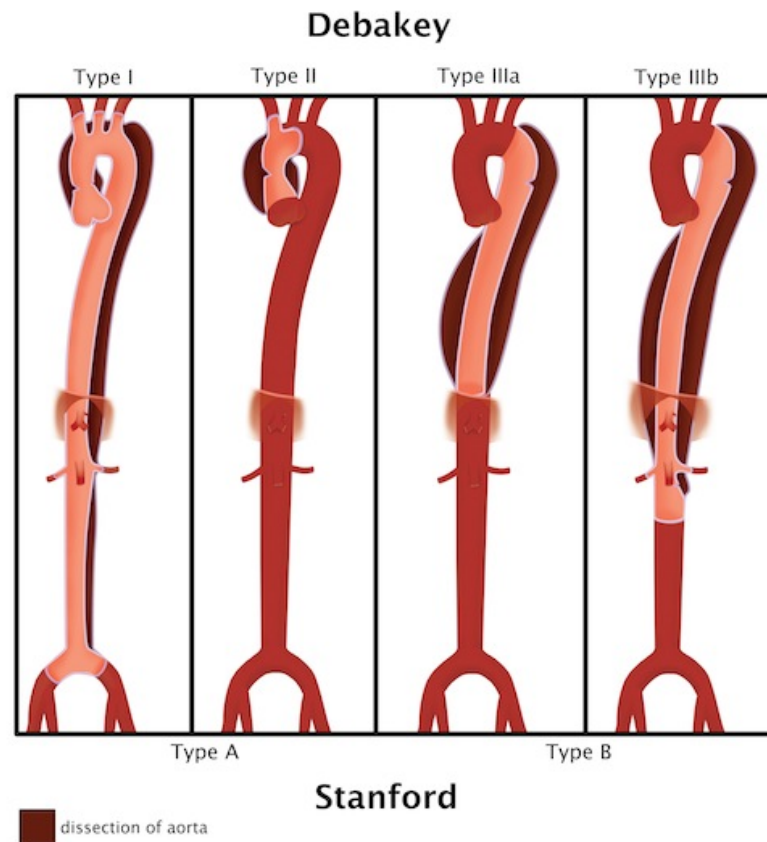
Figure 1.3: Classification of aortic dissection. DeBakey type *I* starts at the ascending aorta with expansion in the entire aorta, while type *II* only effects the ascending aorta. Stanford classification Type A involves both DeBakey types *I* and *II* (any dissection effecting the ascending aorta independent of distal expansion). DeBakey type *IIIa* effects the descending aorta until the visceral segment while type *IIIb* extends up under the diaphragm. Stanford classification Type B involves both DeBakey types *IIIa* and *IIIb* (Ayala and Chen, 2012).

1.4.4 Risk factors & Pathology

The most common predisposing risk factors are structural weakness of the media (cystic media necrosis) and atherosclerosis. As aforementioned atherosclerosis is the reason for flat wall deposits in the intima, which tend to rupture easily. These atherosclerotic ulcer can form the entrance gate of a dissection (Golledge and Eagle, 2008). Certain risk factors for aortic dissection are also arterial hypertension as well as inherited connective tissue disorders such as Marfan syndrome (MFS) or Ehlers-Danlos (EDS) syndrome. Hypertension occurs in 70% of patients. Aortic dissection is the most important cause of morbidity and mortality of pateients with Marfan or Ehlers-Danlos syndromes. Other factors are, for ex-

ample, age between the 6th and 7th decades of life or cocaine abuse. Bicuspid aortic valve can be a problem of cystic medial degeneration, which is often seen in people having an aortic valve with only two instead of three value leaflets (valvulae). Regarding the etiology, mostly young, black, hypertensive men are affected. As a consequence of a surgical intervention it may come to dissection, i.e. aortic valve replacement, bypass, intravascular or cardiac catheterization. Unexplained is the exact context of a dissection during pregnancy in females. About half of all dissections of women younger than 40 years of age occur in the last trimester of pregnancy. Nevertheless, pregnancy has not been reported to be linked directly to aortic dissection. An uncommon aspect is that aortic dissection mostly occurs between the early morning and midday. The frequence is higher in the winter, independent of warm or cold climate conditions (Criado, 2011; Ayala and Chen, 2012; Thalmann et al., 2011).

Improving the understanding about the pathology of aortic dissection is an important step to develop medical treatments to protect patients from diseases affecting the arteries. MFS is a autosomal dominant connective tissue disorder which is mainly manifested in the skeleton, ocular and cardiovascular system. MFS makes arteries prone to dissection. It results from mutations in the FBN1 gene on the chromosome 15q21.1 that encodes the protein fibrillin-1 of the extracellular matrix. Fibrillin-1 is a major component of extracellular microfibrils that can anchor numerous tissues and plays a role in the formation of elastic fibers. Microfibrils are independently found of elastin, but they are also found in combination with elastin that build together the elastic fibers in tissues, like the aorta. Because of structural deficiency of fibrillin-1, microfibrils get weakened (Judge and Dietz, 2005; Golledge and Eagle, 2008). It interacts together with the related fibrillin-2 and other proteins of the ECM, especially elastic fibers, and thus plays an important role in the stability and elasticity of connective tissues. So far over 600 different mutations of the FBN1 gene are described (Moog and Rie, 2014) .

Mutations in the FBN1 gene associated by MFS increase the availability of the transforming growth factor-β (TGF-β). In general, fibrillin-1 protein binds to a large latent complex (LLC). This complex includes the inactive form of he TGF-β. Deficient fibrillin-1 modifies the matrix deposition of the LLC which supports the release of the TGF-β to the extracellular environment. The free and activated form of the TGF-β is a part of different cellular processes, such as growth inhibition, or remodeling inhibitions of the extracellular matrix. TGF-β levels are higher in people with MFS than in healthy ones and thus might serve as a prognostic biomarker for MFS as depicted in a study by Franken et al. (2013). The growth factor TGF-β binds to matrix proteoglycans that affect cell proliferation, cell inhibition, protein synthesis, growth and death. TGF-β contributes to increase or reduce the production of matrix metalloproteases MMPs (Wu et al., 2013). Zhang et al. (2009) described in their article the role of MMPs in the pathobiology of acute coronary syndromes, aortic dissection and aneurysm. MMPs can have effects on any extracellular protein substrates, by activating or degrading them. The expression and activation of some MMPs in aortic tissues that are prone to dilatation and rupture is increased, whereas those of others are decreased. MMPs belong to the family of proteolytic enzymes and are among others,

responsible for the degradation of extracellular matrix proteins in the media, i.e. reduction of smooth muscle cells, fragmentation of collagen and elastic fibers. Tissue inhibitors of metalloproteinases (TIMPs) work against the activity of MMPs and may be a target in treating aortic diseases.

For example, overexpression of different types of MMPs were discovered in unstable atherosclerotic plaque. Also significantly increased MMP-9 concentration and decreased TIMP concentration in patients with aortic aneurysm or dissection. High MMP-9 and MMP-3 values were identified in patients that suffer from hypertension and aortic root dilatation (Wen et al., 2011). MMP-1 is said to be capable of degrading collagen types I, II and III and besides responsible for the initiation of the cleavage of collagen. MMP-2 and MMP-9 degrades type VI collagen and elastin (Wu et al., 2013).

In some cases beta-blockers can stop the progression of dilatation and decrease the risk of dissection and rupture. Every patient with MFS should get an endocarditis prophylaxis if there is an indication. An aortic repair of the ascending part is recommended if the diameter is more than 45 millimeters. In cases of aortic dissection in family the patient can get the surgery earlier (Herold, 2013).

Mass syndrome is a genetic syndrome that is similar the MFS. It is also a connective tissue disorder that involves the aorta, mitral valve, skeleton and skin. To be able to make a diagnosis, at least two of the symptoms have to be present. The causes are said to be mutations in the FBN1 gene (Arslan-Kirchner et al., 2008).

EDS is a rare disease which involves a genetic disorder of collagen synthesis. One distinguishes ten genetic clinical and molecular-biological different types, whereas the autosomal dominant types I-III represent over 80% of all cases. Mutations in genes alter the synthesis and processing of collagen or of proteins that interact with collagen. They thus lead to clinically significant structural changes. Genes that encode fiber proteins are: TNXB, COL1A1, COL1A2, COL3A1, COL5A1 and COL5A2. The connective tissue structure of the skin, blood vessels and joints are insufficiently formed due to the disorder of collagen synthesis. This can lead to a lack of strength, a hyperextensibility of the connective tissue and to a slight tearing of the affected structures, in particular the blood vessels. In patients with EDS operations have a big risk and should be carried out only in case of emergencies (Moll, 1989).

1.4.5 Symptoms & Diagnosis

Aortic dissection symptoms can vary from patient to patient. They can be so nonspecific that aortic dissection is not diagnosed in up to 40% of cases as such (Olin and Fuster, 2003). In the foreground of the clinical symptoms is a sudden onset of chest pain. The progress of the dissection distally causes a change of the pain localization from the front chest region to the neck and later between the shoulder blades. The well-known anamnesis of hypertension, a known thoracic aortic aneurysm or a known Marfan syndrome are always indicators for a dissection (Oberwalder, 2001b). The pain was described by patients as stabbing or ripping and the worst pain they have ever felt. The pain is clearly distinguishably from that

of a myocardial infarction (Akin et al., 2010). The following symptoms are associated with
aortic dissections: sudden onset of chest pain, syncope, limb pain, numbness, weakness,
groin or back pain, shortness of breath and so forth (IRAD, 2014). Clinical investigations
have also shown symptoms like pulmonary edema, hypertension or hypotension. In less
than 20% of all patients a reduced pulse rate was noticed. Neurological malfunctions are
also significant due to obstruction of the carotid artery or spinal cord ischemia. In the
event of a propagating dissection there may be an aneurysmatic dilatation, that can cause
to Horner syndrome, superior vena cava syndrome, dysphagia, hoarseness or obstruction
of the respiratory tract. Typical signs of a proximal rather than a distal dissection are pulse
deficits, neurological manifestations and the murmur of aortic regurgitation (Dietel et al.,
2005; Ayala and Chen, 2012).

The notice of a dissection flap between two separate lumen is a sure indication of an
aortic dissection. To confirm dissection the diagnosis can be realized either with contrast-
enhanced angiography or noninvasive techniques such as chest x-ray, echocardiography,
computed tomography (CT) or magnetic resonance imaging (MRI). The aortic angiography
can show the entry point, the intimal flap and the false as well as the true lumen. Also,
one can see the propagation of the dissection in large arteries. The sensitivity of aortic
angiography for detecting an intimal flap is about 70%, for detecting an intimal tear about
56% and for the false lumen about 87%. A transthoracic echocardiography has a sensitivity
of 60% up to 85%. The use of chest x-ray is limited by the low sensitivity of 64% and
specificity of 86% (Ayala and Chen, 2012; Dietel et al., 2005).

Contrast-enhanced helical CT has a sensitivity of 100% and a specificity of 98%, and is
thus the most commonly used technique for the detection of an aortic dissection. The most
accurate imaging modality with a sensitivity of 100% and a specificity of 94% is MRI. CT
and MRI are well suited for the detection of intramural hemorrhage and penetrating ulcers.
A special feature of MRI is that the direction of the blood flow can be detected, in order
to discern whether the blood flow and thus also the dissection is antegrade or retrograde.
Nevertheless, MRI technology is of limited value for diagnosing acute aortic dissection,
because it can neither be used for hemodynamically unstable patients, nor in patients with
implanted metal devices and it takes to much time to receive the images (Ayala and Chen,
2012; Dietel et al., 2005).

1.4.6 Treatment

In the event that an aortic dissection is confirmed, rapid drug treatment should be started.
Any patients affected need to be looked after at a monitoring station with intensive mon-
itoring of hemodynamics and excretion of urine. For diagnosed hypertension, a therapy
should be started in order to reduce the cardiac contractility as well as the systemic arte-
rial pressure to avoid shear forces. Therefore, parenteral beta blocker are administered,
which include medications such as labetalol and metoprolol to achieve a target heart rate
of between 50 and 60 beats per minute. Moreover, with the aid of infusions of sodium
nitroprusside a reduction of systolic blood pressure to a maximum of 120mmHg can be

reached. Pain should be controlled with morphine (Akin et al., 2010; Dietel et al., 2005). The decision whether a surgical intervention is necessary or medical treatment is sufficient depends on the type of dissection. Regardless of the type of dissection an operative indication exists if the diameter of the aorta has a critical size from 5 to 5.5 centimeters. For an uncomplicated and stable distal dissection (type B), the patient is usually treated with medications only. Surgery is not intended in this case unless complications occur. Surgical treatment is necessary in case of dissection of the ascending aorta (type A) and complicated type B dissections. The latter is characterized by the participation of main branches of the aorta, by a threat of rupture, evidence of further dissection or a persistent pain. In terms of complicated type B dissections, the presence of a Marfan's syndrome or a resulting malperfusion of major organs are also reasons for a surgical intervention. To avoid the dissection from rupture is the main objective of a surgical intervention. The involved region is resected and then replaced by a interposition graft. If the aortic valve is also affected by the dissection, a composite valve prosthesis is used. The graft is glued and sutured to the residual ends of the artery. The replacement prostheses are normally made of woven dacron tissue, which is coated with collagen for tightness. An approved treatment alternative is the use of aortic stent-grafts in type B dissection. The goal is to close the tear that dissected under usage of a tube-like nitinol grid stent to induce thrombosis in the false lumen and restoring a functional aortic wall. According data of the IRAD (2014) (Internation Registery of Aortic Dissection) patients have better survival rates after endovascular treatment than in case of open surgical repair. Despite emergency open surgical repair, aortic dissection has a total mortality risk of 15% to 20% in the hospital. Frequent reasons for this are pulmonary embolism and heart attack. Patients with an aortic dissection have to undergo a long term therapy. Thereby a variety of vital parameters are checked periodically. As mentioned in Dietel et al. the survival rate for the first decade is about 60% and therefore considered to be good (Dietel et al., 2005; Akin et al., 2010; Oberwalder, 2001b).

2 Materials & Methods

In this section the main steps performed on the utilized human thoracic aortic tissue, i.e. the required specimen preparation, the experimental setup of the individual tests and the applied testing protocols, are described. There is also an introduction of the mechanical theory and appropriate equations for the evaluations of uniaxial tension tests and triaxial shear tests.

2.1 Materials

In this Master Thesis twelve aortas at different states, i.e. dissected, aneurysmatic or healthy, were investigated. All human aortic tissues which were used for test purpose as part of this work were provided from the Department of Cardiac Surgery, Medical University of Graz, and from the New York University School of Medicine. The authorization to use autopsy material from human subjects was approved by the Ethics Committee, Medical University Graz, Austria.

The human aortic tissue was removed from patients during surgery and then immediately sent to the Institute of Biomechanics (Graz University of Technology) in order to keep the duration of autolysis as low as possible. The aortic tissue was transported in a small container filled with a phosphate-buffered physiological saline solution (PBS). For more details see section 2.2. In the case that the tissue was sent from the New York University School of Medicine a small tube was used containing cryopreserving solution. The tube was placed in a styrofoam container filled with dry ice in order to cool the tissue during shipping. After receiving the human aortic tissue, if the sample was tested immediately, it was kept in the refrigerator at 4°C in PBS solution to prevent tissue of phenomena like tissue necrosis and drying out. The samples that were not investigated within the next 48h were stored at -25°C in a freezer until testing, maximum for two weeks. According to the size of the tissue as many tests as possible were performed in order to increase the reliability of the data.

In Fig. 2.1 a dissected thoracic aortic tissue of sample *II* is presented. It shows a section of the human thoracic aorta as it was extracted during surgery with its detached adventitia of the media and the intermediate thrombus, which are formed following dissection. It was taken particular care to ensure that the tissue contained no atherosclerotic plaques. This was necessary to avoid any bias of the data. Figure 2.2 shows the aorta of sample *VI* containing plaques which occur as a part of atherosclerosis. In Table 2.1 information about the anamnesis of the donors from which the specimens *I – XIII* were obtained are listed. Additionally operation date, race, ethnicity and the position, where the specimen

were harvested, are provided. In section 4, the anamnesis of the donors are compared with their mechanical properties.
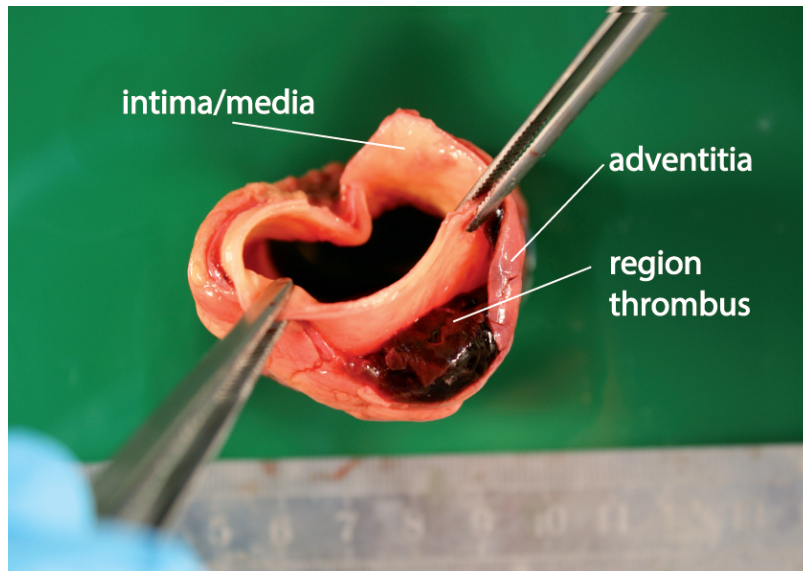
Figure 2.1: Representative photograph of the human sample *II* containing a thrombus as a result of aortic dissection.
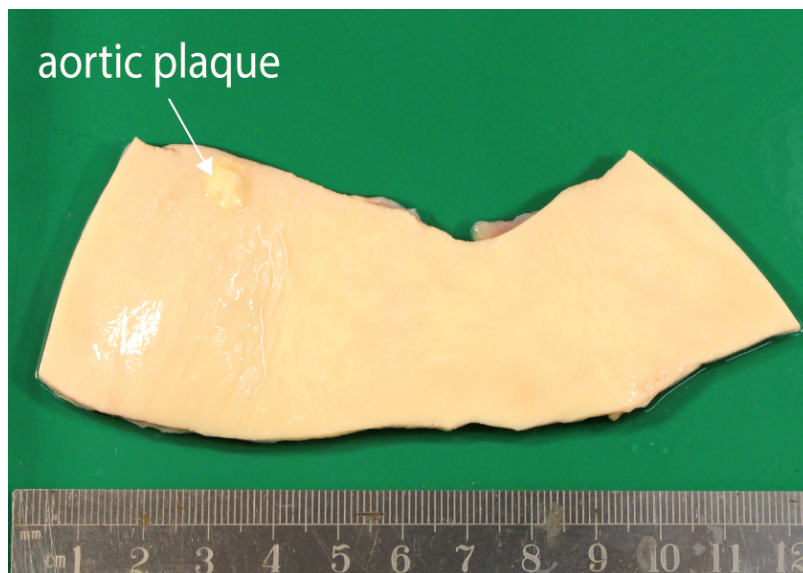
Figure 2.2: Representative photograph of the human sample *VI* containing an aortic plaque. The aorta was cut open along the axial direction z.

Table 2.1: Donor information, such as age gender and primary disease. Furthermore, the conditions of the aortas with regard to the stage of atherosclerosis are shown. Connective tissue disorders and risk factors if they are known such as other abnormalities are also provided.

	Specimen No.												
	I	*II*	*III*	*IV*	*V*	*VI*	*VII*	*VIII*	*IX*	*X*	*XI*	*XII*	*XIII*
Institute	*NYU*	*MUG*	*MUG*	*MUG*	*MUG*	*MUG*	*NYU*	*NYU*	*MUG*	*NYU*	*MUG*	*NYU*	*NYU*
Age, yr	43	65	56	58	71	71	52	64	50	28	71	72	62
Gender	*M*	*M*	*F*	*M*	*M*	*M*	*M*	*M*	*M*	*F*	*M*	*F*	*M*
State	*DI*	*DI*	*AN/H*	*DI*	*AN*	*AN*	*AN*	*AN*	*AN*	*AN*	*DI*	*AN*	*AN*
Position	*DA*	*AA*	*AA*	*AA*	*AA*	*AA*	*ARA*	*AA*	*AA*	*DA*	*AA*	*DA*	*DA*
Tissue dis.	−	−	*FD*	−	−	−	*MF/MA*	−	−	*MF*	−	−	−
Ath.stage	−	*AS*	−	*AS*	*AS*	*AS*	−	−	*AS*	−	−	−	−
BP	108/64	−	−	−	−	−	143/85	125/73	−	−	−	−	−
Risk	*HT*	*HT*	*HT*	*HT*	*HT*	*HT*	*HT/HL*	*HT*	*HT*	*HT*	−	*HT*	*AS/AI*
factors	*SM*	−	*SM*	−	−	*HL*	*COPD*	*HL*	*HL*	*PTAA*	−	*HM*	−
							OB		*OB*				

AN, aneurysm; AA, ascending aorta; AS, atherosclerosis; BP, blood pressure (post-operative); DA, descending aorta; DI, dissected; F, female; H, healthy; FD, fibromyxoide degeneration; HM, heart murmur; HL, hyperlipidemia; HT, hypertension; M, male; MF, marfan syndrome; MA, mass syndrome; MUG, Medical University Graz; NYU, New York University; OB, obesity; PTAA, previous thoracic aortic aneurysm; SM, smoker

2.2 Chemical solutions

Chemical solutions were used for the transport, testing and storage of thoracic aortic tissue. The physical properties of materials depend on environmental factors such as e.g. temperature and chemical composition of the surrounding medium. The human body tries to maintain its chemical-physical milieu at a constant level to ensure a defined and optimized operation of its organs that is called homeostasis. This includes constant values of ion concentrations, pH-value, oxygen partial pressure, carbon dioxide partial pressure, temperature, etc. For this reason the measurement of physical properties of human tissue should be done under the following conditions:

- No gassing with oxygen (O_2) or carbon dioxide (CO_2)

- Temperature of testing solution 37°C

  The temperature of the testing solution should correspond to the *in vivo* conditions. The mechanical properties of human tissue under physiological loads are in the range of 24°C–39°C and are assumed to be largely constant (Kang et al., 1995). It is important that a temperature of 41°C must not exceed, because above this temperature, proteins start to get denaturated, i.e. changed their structure (Chen et al., 1998). Differences in temperature of 1°C, have hardly any influence.
  In order to ensure stable experimental conditions the temperature of the testing solution was maintained with a heating coil. Inside the heating coil distilled water was pumped by a thermostatically controlled heating bath. The temperature of the testing solution was checked regularly with a rod thermometer.

- Useage of phosphate-buffered saline (PBS) solution

  For handling the individual steps (transport, storage and testing) of testing human thoracic aortic tissues a PBS solution was used.

  PBS is a water-based salt solution, it is suitable to maintain a constant pH-value (approx. 7.2–7.4). PBS is non-toxic to cells and the ion concentration and osmolarity are based on the human body milieu. The major advantage is that it prevents tissue-drying. Here, PBS was used for the transport, storage and experimental testing of the different tissues.
  The solution was prepared at the Institute of Biomechanics (Graz University of Technology) and used the following quantitative composition.

  - 1.44 g $NaH_2PO_4 + 2H_2O$
  - 0.24 g KH_2PO_4
  - 0.2 g KCl
  - 8 g $NaCl$
  - dissolved in (distilled) 1000 ml H_2O

In the case that the tissue sample was sent from the University School of Medicine (New York), a PBS like solution was used with an addition of 10% Dimethylsulfoxide (C_2H_6OS).

As a solution for fixation of tested specimens and storage 4% Formaldehyde (CH_2O) was used. This was used for chemical fixation of the tissues for microstructural investigations.

2.3 Specimen preparation

At first, the loose connective tissue and adipose tissue attached to the surface of the adventitia was removed. Subsequently, the tubular aorta was cut along the axial direction to obtain a flat and rectangular sheet. The three layers of the aorta had to be separated from each other. Therefore it was necessary to find a starting point where the layer separation process could be easily accomplished. By utilization of surgical tools such as a scalpel and tweezers the inner layer (intima) and the outer layer (adventitia) were separated from the middle layer (media), see Fig. 2.3. In addition a magnifying glass was used to ensure accurate work. It was difficult to separate the layers, resulting in an imperfect dissection, but only small fractions of the media were found attached to the adventitia. The effect of imperfect layer separation on the mechanical behavior can be neglected.

Throughout the preparation process the medial tissue was regularly immersed with PBS solution to protect the medial tissue against drying. For fixing the specimen on the testing device cyanoacrylate adhesive glue (Loctite®: Super Kleber, Power Gel) was used. It is a non-penetrating glue in order to prevent falsification of tissue strength, stiffness and non-linearity. The additional individual specimen preparation which has been required for the individual tests (uniaxial tension, triaxial shear tests, etc.) are described in the following sections.

Thickness measurement

The information of the geometrical dimensions of each specimen was particular important for every type of mechanical testing. The thickness of the samples was measured by means of a video extensometer to ensure accurate detection. The CCD-camera was calibrated before measurements. This process took place in the air and was realized by an object slide with 1mm in thickness, which sides were colored with a black marker. The sample was placed on the object slide so that their edges coincided. Finally, the thickness of the sample was optically measured. The thickness was obtained by subtracting the thickness of the object slide from the average contour thickness along the gage region of the sample. For a more detailed explanation see the study by Sommer et al. (2008).
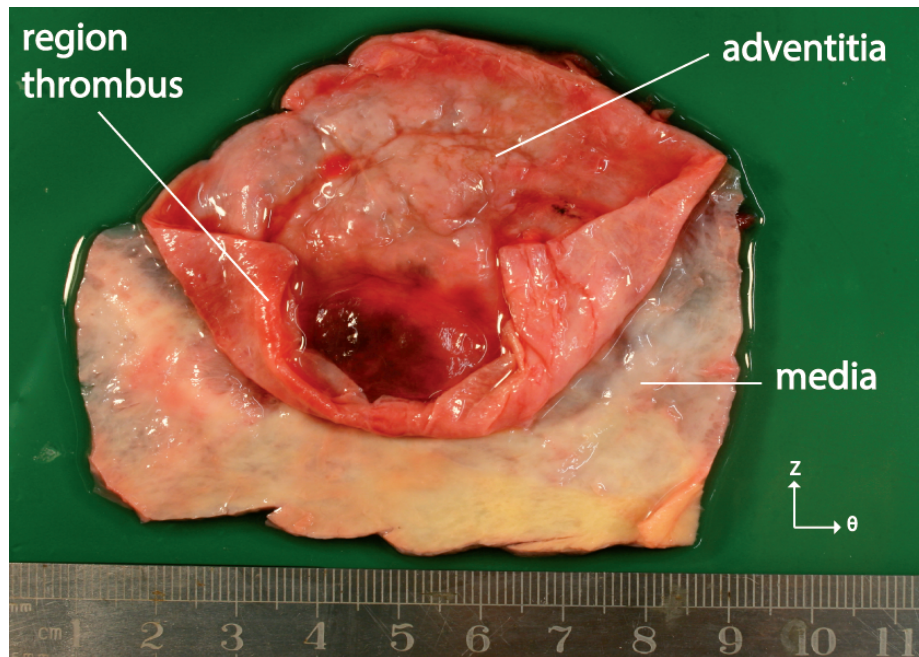
Figure 2.3: Arterial layers (adventitia and media) prepared from a dissected aortic patch, donor sample *X*. In the center, a blood thrombus is visible that formed during aortic dissection. The circumferential and axial directions of the artery are indicated by θ and z, respectively. The photographed centimeter scale provides a dimensional reference.

2.4 Experimental setup

2.4.1 Uniaxial tension testing device

Uniaxial tension rupture- and direct tension tests were performed with a computer-controlled, screw-driven and high-precision uniaxial tension testing machine, μ-Strain Instrument ME 30-1. The machine was manufactured by the company Messphysik, Fürstenfeld, Austria. It was designed for small biological specimens. The machine drive is controlled by an external controller (EDC 25/90 W, DOLI, München, Germany) and the position control resolution was specified by the manufacturer as 0.04μm of the upper and the lower crosshead of the tension testing machine, see Fig. 2.4. For measuring the tension forces a 10N Class 1 strain gauge-load cell (type TCA 10N, code CTCA1K5; AEP transducers, Modena, Italy) was used, which was mounted on the upper cross head. The load cell accuracy is stated as 0.02% of the measured value. It is evident that in the worst case a combined error of 0.6mN might occur at a maximum force of 2N.

In case of uniaxial tension strength measurements, the specimens were examined inside a perpex container filled with PBS which was maintained at a constant temperature of 37°C ±1.0°C by a heater-circulation unit (type Ecoline E 200; LAUDA, Lauda-Koenigshofen,

Germany). With a PC-based CCD-camera videoextensometer it is possible to measure gauge length and width of the specimen optically. A schematic drawing of the setup is shown in Fig. 2.5.

For the fixation of the samples on the testing machine for the uniaxial rupture tests a plastic rod with clamps and a metallic jig were used, while in the case of direct tension test two specially manufactured cylindrical plastic rods were used as specimen holders. A schematic drawing of specimen fixation between the two rods is shown in Fig. 2.6.

For a more accurate description of the components see Sommer (2010). All tests were conducted with the PC-based application software "Kunststoffzugversuch".
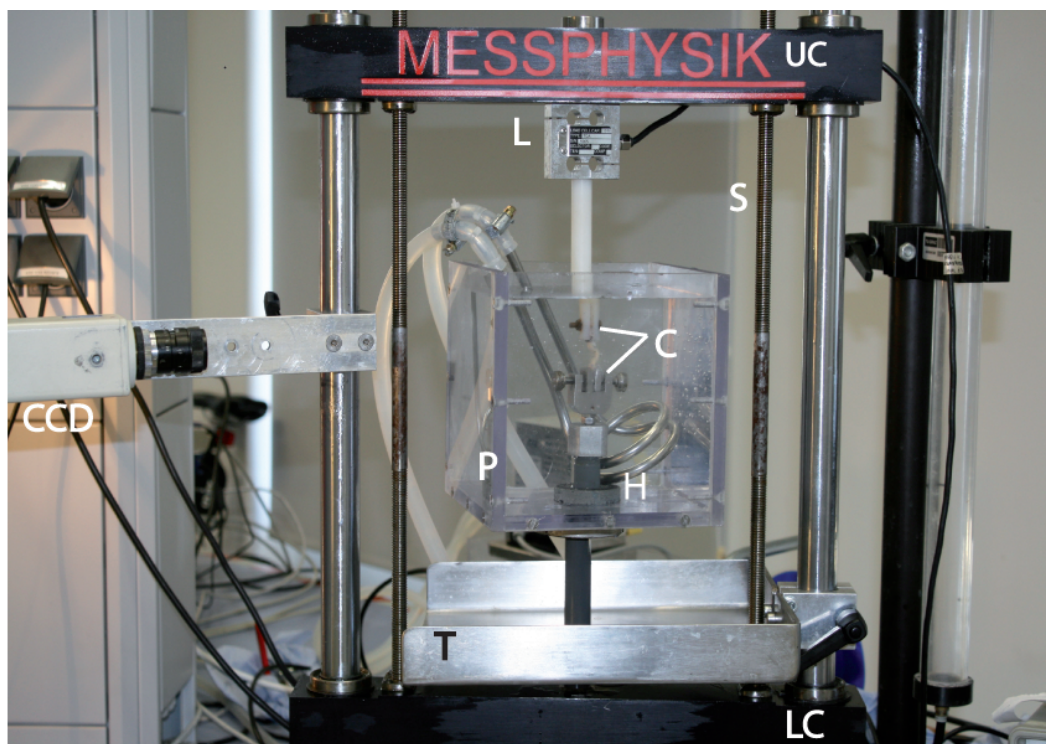
Figure 2.4: The uniaxial testing apparatus for the uniaxial tension tests.
CCD, CCD-camera; C, clamping heads; S, drive spindle; H, heating spiral; L, load cell (force measurement unit); LC, lower crosshead; T, metal table; M, motor; UC, upper crosshead; P, perpex container
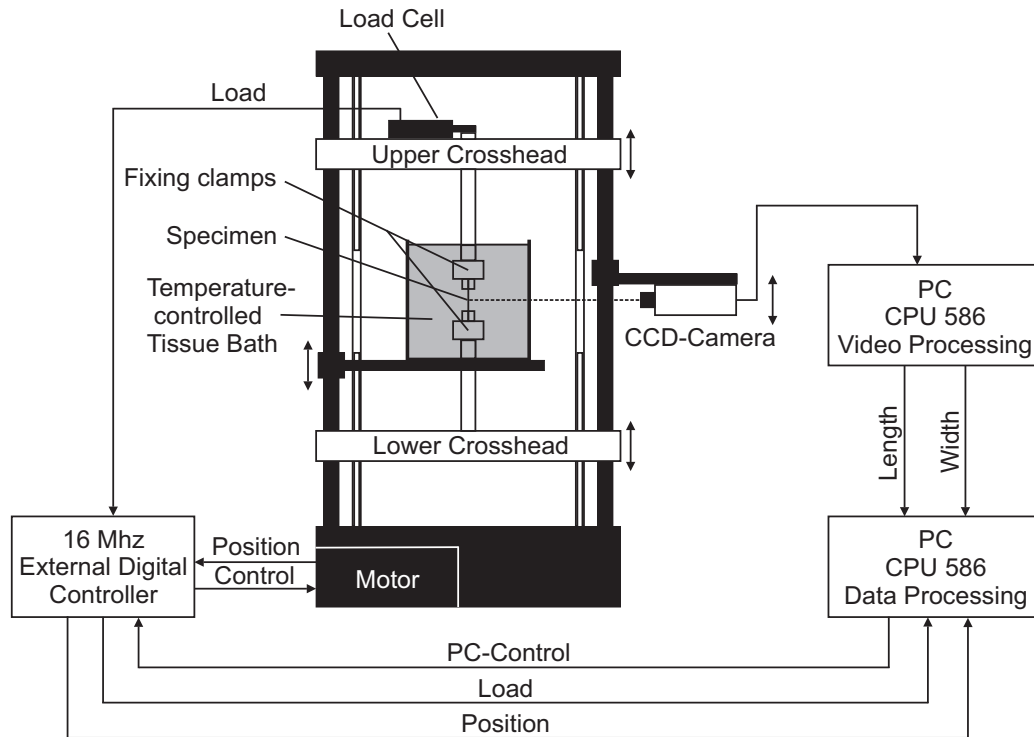
Figure 2.5: Schematic experimental setup adapted fromSommer et al. (2008).
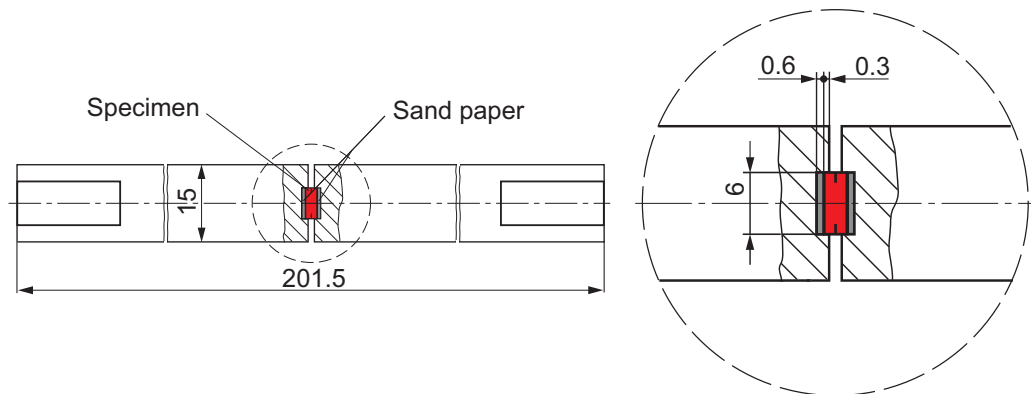
Figure 2.6: Schematic drawing of specimen fixation between the plastic rods (direct tension test). Dimensions are given in millimeters. Adapted from Sommer et al. (2008).

2.4.2 Triaxial testing device

For the investigation of shear properties of aortic tissue a triaxial shear testing device was used as shown by an schematic illustration in Fig. 2.7. A representative photograph is also depicted in Fig. 2.8 (Messphysik, Austria). The machine has been adapted to perform shear deformation of highly deformable soft biological tissues by the Institute of Biomechanics (Graz University of Technology, Austria). The device has an upper platform which is moveable in the z-direction and a lower platform movable in the x- and y-direction. The lower platform is moved relative to the fixed upper platform using a biaxial translation stage. The system operates with a stroke resolution of 0.25μm in the x- and y-directions and of 0.04μm in the z-direction. The machine contains a 3-axis force-sensor (K3D40, ME-Measuring Equipment, Henninsdorf, Germany) which makes it possible to measure the three orthogonal forces in the three directions x, y and z. A capacity of ±2N and a linearity error of 2% between 20mN and 2N of the force sensor are specified by the manufacturer. Furthermore, the cross-talk between the x- and y-axes of the force sensor is specified to be less than 0.5%, whereas the crosstalk between the z- and x-y-axes is specified to be less than 1% by the manufacturer. The software TestXpert II (Version 3.2 by Zwick & Roell GmbH & Co. KG, Ulm, Germany) on a Windows-based personal computer, which is associated with the machine is used for data acquisition and motor control.
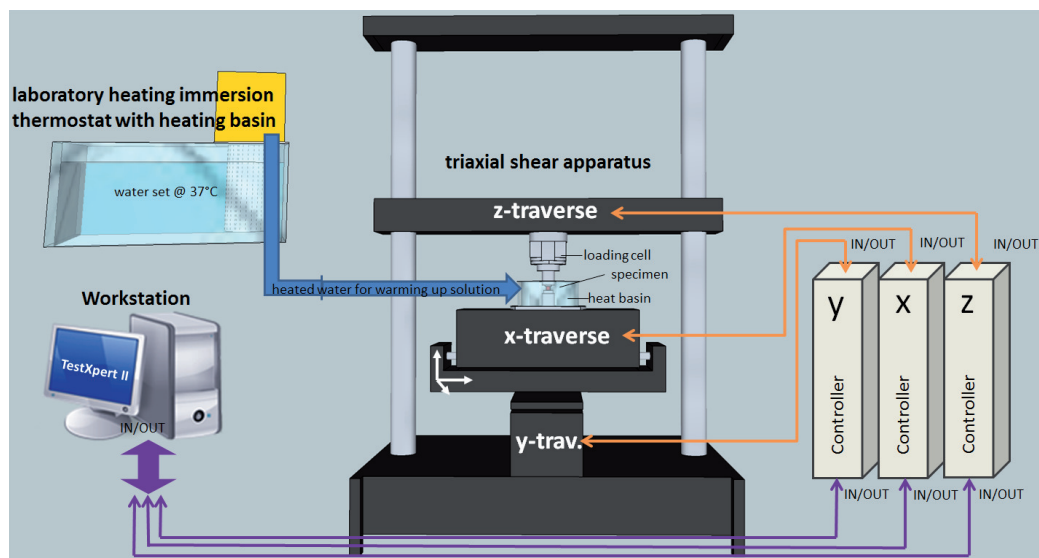
Figure 2.7: Illustration of the triaxial shear testing device taken from Kutschera (2012).
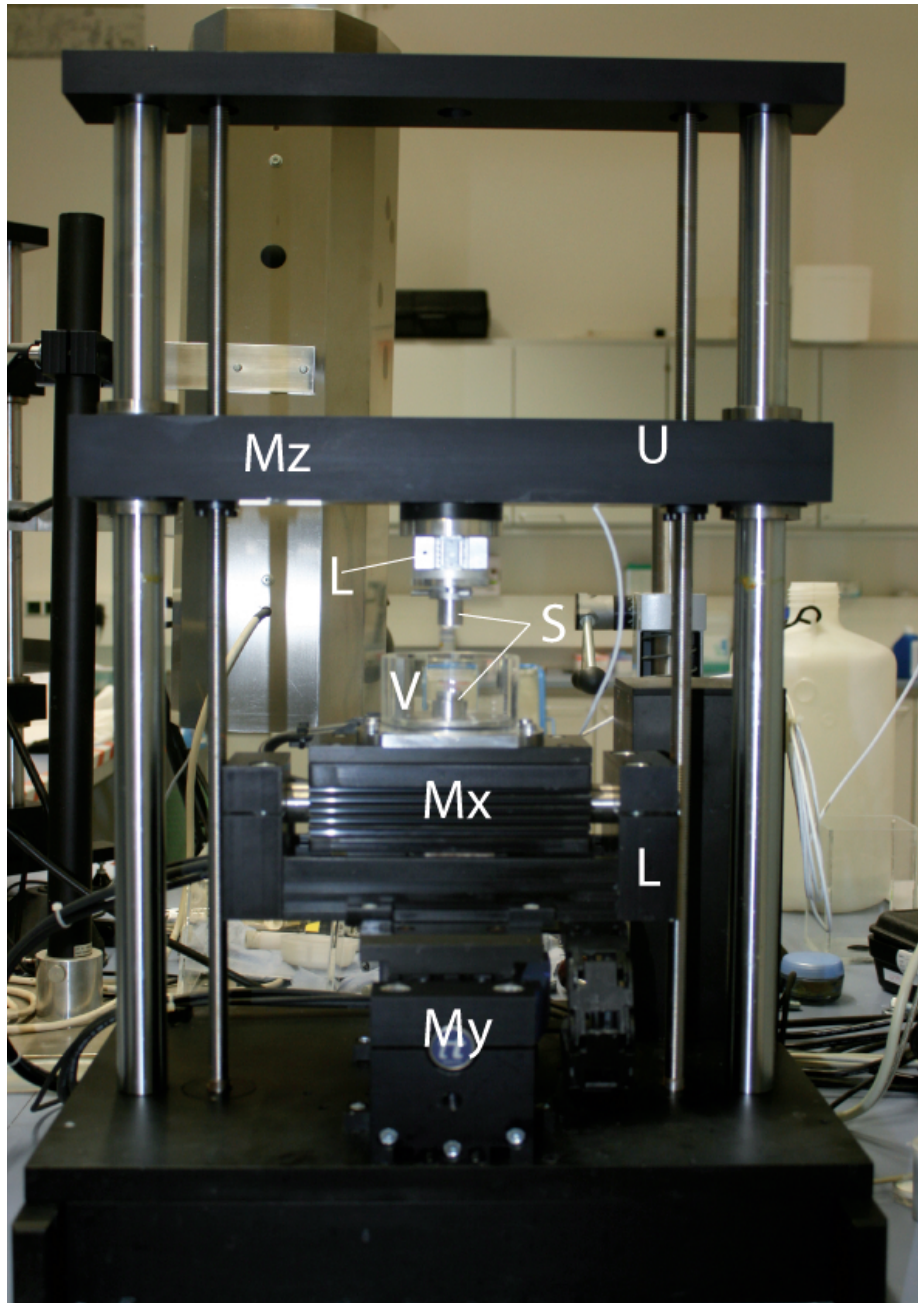
Figure 2.8: The triaxial testing apparatus with its components. L, lower platform; L, triax-
ial loading cell (force measurement unit); Mx, My, Mz – linear actuators in x,
y and z; S, metallic "stamps"; U, upper platform; V, glass vessel

2.5 Direct tension test

2.5.1 Specimen preparation

For the execution of the direct tension tests a special specimen form was used as described in Sommer et al. (2008). The specimens were punched out with a cylindrical blanking tool. The coin-shaped specimen for the direct tension test had a diameter of 6.0mm and a specific thickness. The geometrical dimensions of the thickness of the different specimen are shown in Table 2.2.

To complete the final preparation of the specimen an incision of about 1.0mm around the circumference of the circular specimen was made. The cut was made with a specially prepared surgical knife with the intention for the initiation of a predetermined breaking point and thus a better control of propagation of tissue failure. Figure 2.9 shows a sketch of a cylindrical coin-shaped specimen. As a result, the diameter of the sample was reduced by 2mm. In the next step, a small strip of sandpaper was adhered to the upper and lower surface of the sample. In particular, the use of sandpaper leads to a stronger connection between the specimen and plastic rods which results in an increase of the success rate of the direct tension tests.

Table 2.2: Sample numbers and thickness values before direct tension test.

Specimen No.	I	II	III	IV	V	VI	VII	VIII	IX	X	XI	XII	XIII	mean value $\pm$ SD
Thickness (mm)	2.3	1.75	1.9	1.9	1.7	1.6	2	2.1	1.8	2	1	1.8	1.9	1.83 ± 0.30
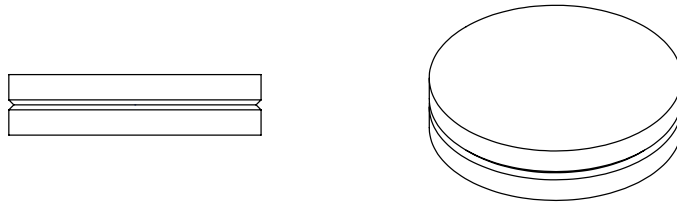
Figure 2.9: Sketch of a direct tension test specimen, a circular punch-out throughout the radial direction of the artery with an additional incision around the circumference to induce failure.

2.5.2 Testing procedure

At first, the coin-shaped specimen with the sandpaper on both sites was glued on one of the plastic rods which was used as specimen holder, and then mounted on the upper crosshead of the uniaxial testing machine. Furthermore, super adhesive glue was placed on the lower rod. At this point zero-load of the tension force was defined. The two plastic rods were moved together manually with the force generation component, so that a compression force between 0.5 and 1.0N was applied to the specimen for about 4 minutes, so that the super adhesive had enough time to harden. Thereafter, the two plastic rods were moved apart manually to the previously defined zero-load of the tension force. Before testing, the aortic tissue was moistened with PBS to protect the tissue from drying. Direct tension tests were conducted in the environment of air, because they could be conducted within a short time frame within one minute.

2.5.3 Testing protocol

The testing software of the direct tension test required a drive apart of the upper and lower transverse of the machine. The tension forces acting on the sample between the plastic rods, caused the tearing apart of the coin-shaped tissue. The extension rate for all the tests was selected as 1mm/min, to bring the tissue as smoothly as possible until the failure stress. The measured values for the direct tension test were time, force and displacement. These data of every test were stored in a *.dat* file. From the recorded measurement data, Cauchy stress vs. stretch diagrams were generated. In Fig. 2.10 a photograph during a successful direct tension test is depicted.
In order to calculate the radial failure stress of the direct tension test Eq. (2.1) is used.

Figure 2.10: Example illustration of the end stage of a successful direct tension test.

$$\sigma^u = \frac{F_{\mathrm{max}}}{A} = \frac{F_{\mathrm{max}}}{\frac{\pi}{4}d_1^2} \qquad (2.1)$$

σ^u ...   ultimate radial failures stress   [N/mm^2 = MPa]
F_{max} ...   max. tension force   [N]
A ...   initial cross section area   [mm^2]
d_1 ...   diameter of the specimen   [mm]

To compute the Cauchy stress, the stretch λ has to be included in calculation Eq. (2.1) as shown in Eq. (2.2) below:

$$\sigma = \frac{f}{A} \cdot \lambda = \frac{f}{\frac{\pi}{4}d_1^2} \cdot \frac{d_2 + p}{d_2} \qquad (2.2)$$

σ ...   cauchy stress   [N/mm^2 = MPa]
f ...   actual tension force   [N]
A ...   initial cross section area   [mm^2]
λ ...   stretch   []
d_1 ...   diameter of the specimen   [mm]
d_2 ...   thickness of the specimen   [mm]
p ...   displacement   [mm]

The Cauchy stress σ results from the quotient of the actual tension force f and the initial cross section area A of the coin-shaped specimen multiplied by the stretch λ. The unit for the Cauchy stress is thus N/mm^2.

2.6 Uniaxial tension test

2.6.1 Specimen preparation

For the uniaxial tension test a special punching tool was used for the preparation of the specimens. The bone shaped punching tool has on both ends a width of 9.5mm and in the middle a restriction of 4mm. This restriction results in a failure of the tissue in the center of the specimen. For each aorta a separate specimen was cut out in both longitudinal and circumferential direction. Representative sketches of the shape of the specimen used for uniaxial tension test are depicted in Fig. 2.11.

It was necessary at both sides of the specimen to glue rectangular pieces of sandpaper with super adhesive glue. This design was required to ensure proper clamping in the tension testing machine and to avoid that the sample tears out from the clamps of the machine during loading.

Moreover, in order to measure the deformation, it was required to add two black colored markers (sponge rubber) to the specimen. These were glued transversely in parallel on the surface of the tissue and used as gauge markers for the deformation measurement. The distance between the two markers was approximately four millimeters.

(a)   (b)
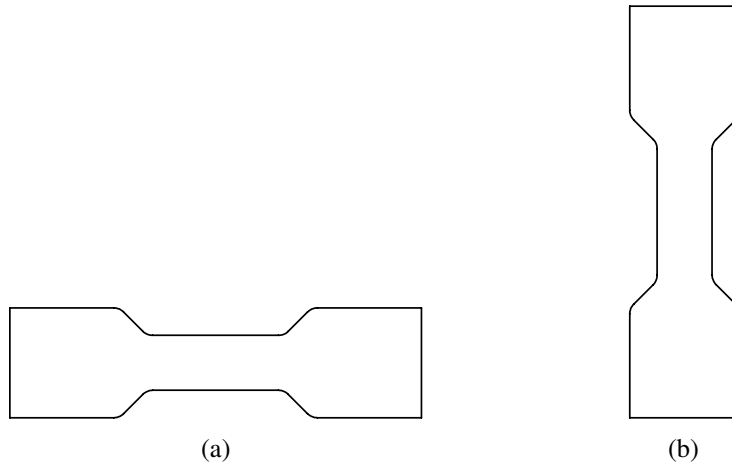
Figure 2.11: Sketch of uniaxial tension test specimens: (a) bone shaped specimen in circumferential and (b) in longitudinal direction.

2.6.2 Testing procedure

Before testing, it was required to calibrate the videoextensometer. Following steps had to be performed.

- Clamping of the calibration standard in the machine

- Checking of the camera settings:
  The CCD-camera was aligned perpendicular to the samples normal axis to reach a normal projection. This results in a consistent image sharpness and width over the whole sample length.

- Useage of the smallest camera's aperture to achieve a high depth of focus

- Focusing of the camera

- Removing bubbles and cleaning the entrance window of the cuvette and the camera lense

- Optimizeing the lighting:
  Attach white paper on the opposite side of the camera at the cuvette, in order to increase the contrast between the sample and its environment. Beyond this, the setup is

illuminated from both sides and the room is darkened, to ensure that the experimental conditions are independent of the time of day.

- Starting calibration:
  The field of view of the camera was calibrated by a special tool for dimension measurements of the specimens.

- Finally, saving of the calibration parameters

The samples were tested inside a perspex container, which was filled with PBS solution. A heater-circulation unit kept the temperature of the solution constant at $37°C \pm 1.0°C$, checked by a thermometer. During heating of the solution, small air bubbles formed around the specimen. To avoid errors they were removed by the use of a paintbrush.

The specimen was mounted between the clamps. After being attached to the upper transverse arm, the zero-load was defined. To accomplish that the perspex container was moved up to a certain point and the displayed tension force was set to 0N. The buoyancy of the medium was compensated by this. If the displayed tension force is still 0N after mounting the specimen to the lower rod and moving up the perplex container to the certain point the specimen was mounted without an prestress.

The perspex container was positioned in a way that the sample was completely immersed in PBS. The CCD-camera was aligned perpendicular to the sample normal axis, in a way that it was possible throughout the entire experiment to record the process. The background of the specimen had to be black to get a better contrast between the almost white sample and its environment. Additional lighting were installed for a better contrast.

2.6.3 Testing Protocol

Before the rupture test was started it was necessary to perform preconditioning of the arterial tissue. The purpose of preconditioning was explained in Sec. 1.3.5 or in the study by Holzapfel et al. (2005). For every specimen, five loading/unloading cycles were performed. A force driven protocol was employed, where the maximum tension force was estimated in relation to the reference area of the specimen. The crosshead speed for the pre-conditioning cycles was chosen to be 2mm/min. Figure 2.12 shows a representative example of the tissue preconditioning behavior. Five cycles for pre-conditioning the tissue up to 50kPa were performed. The behavior of the mean fiber direction is quite similar to the cross-fiber direction in terms of preconditioning, therefore the latter is not shown here. The hysteresis of the first preconditioning cycles in Fig. 2.12 were always larger than the subsequent ones.

Immediately after preconditioning the uniaxial rupture test was conducted. The upper and the lower fixing clamps of the testing device moved apart until the tissue ruptured. The specimen and its gauge region were always in the same field of view. Similar to the direct tension test, the testing machine was operated with a speed of 1mm/min, whereby the tissue
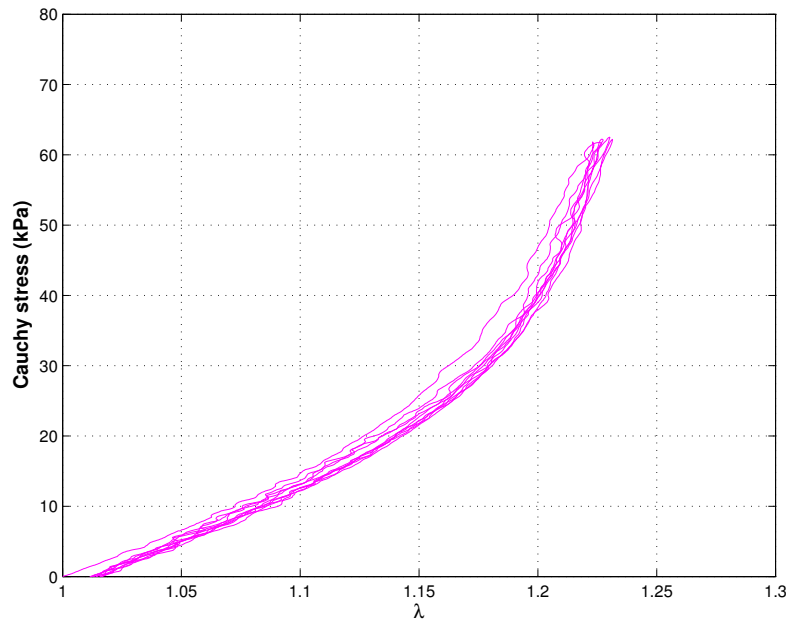
Figure 2.12: Preconditioning behavior of a human thoracic medial aorta (up to a stress level of 50kPa) in the longitudinal direction of donor *XI*.

was loaded up to failure. The applied force that led to failure is defined as the fracture force and is measured in Newton (N). Time, force and displacement were continuously recorded. By the use of a CCD-camera (videoextensometer), it was possible to measure the actual width and the actual length (gauge length) change between the sponge rubber markers in real time. All these data were saved in a *.dat*-file. For better perception concerning the measurement of the two parameters (actual width and actual length change), screenshots during the measuring process are shown in Figs. 2.13 and 2.14.

During the testing procedure it was not possible to measure the change of the actual thickness of the specimen. The actual thickness is necessary to obtain the Cauchy stress. Cauchy stresses were calculated under the assumption of incompressibility of soft tissue and therefore, the volume does not change under mechanical load as shown in Eq. (2.3).

With the aid of incompressibility, it was possible to calculate the relation of the Cauchy stress and stretch, as can be seen in Eq. (2.4) below.

After the uniaxial tension test has been successfully completed, the specimen was inserted in 4% formalin-solution for fixation and further histological evaluation. A sample ready for testing is shown in Fig. 2.15 (a) while Fig. 2.15 (b) depicts a representative photograph of a successfully ruptured specimen. The individual ultimate tension stresses and the related ultimate streches for the individual tests are indicated in Table 3.3.

$$V = L \cdot W \cdot T = l \cdot w \cdot t = const. \longrightarrow t = \frac{L \cdot W \cdot T}{l \cdot w} \qquad (2.3)$$

V	...	Volume	[mm^3]
l	...	actual length	[mm]
L	...	initial length	[mm]
w	...	actual width	[mm]
W	...	initial width	[mm]
t	...	actual thickness	[mm]
T	...	initial thickness	[mm]

$$\sigma = \frac{f}{a} = \frac{f}{w \cdot t} = \frac{f}{T \cdot W} \cdot \frac{l}{L} \longrightarrow \sigma = \frac{f}{T \cdot W} \cdot \lambda \qquad (2.4)$$

σ	...	Cauchy stress	[N/mm^2 = MPa]
f	...	actual tension force	[N]
a	...	actual cross section area	[mm^2]
λ	...	stretch	[]

The Cauchy stress σ is thus the result of the division of the actual tension force f and the actual cross section area a (actual width w · actual thickness t) of the specimen and is measured in N/mm^2. As aforementioned, the actual thickness t of the specimen could not be measured, that is why it is substituted from Eq. (2.3) to calculate the Cauchy stress σ vs. stretch λ.

Ultimate tension stresses $\sigma_{\theta\theta}^u$ and σ_{zz}^u were determined in the circumferential and the axial direction, respectively. Ultimate tension stress and the associated ultimate stretch ratio λ^u for the individual rupture tests are calculated by the experimentally determined fracture tension force f_{f}.

Ultimate tension stress is characterized by the maximum resistence to fracture. In order to calculate the ultimate tension stress $\sigma_{\theta\theta}^u$ and σ_{zz}^u the following Eq. (2.5) is applied.

$$\sigma^u = \frac{f_{\mathrm{f}}}{W \cdot T} \cdot \frac{l}{L} = \frac{f_{\mathrm{f}}}{W \cdot T} \cdot \lambda^u \qquad (2.5)$$

σ^u	...	ultimate tension stress	[N/mm^2 = MPa]
λu	...	ultimate stretch ratio	[]
f_{f}	...	fracture tension force	[N]
W	...	initial width	[mm]
T	...	initial thickness	[mm]
l	...	actual length	[mm]
L	...	initial length	[mm]
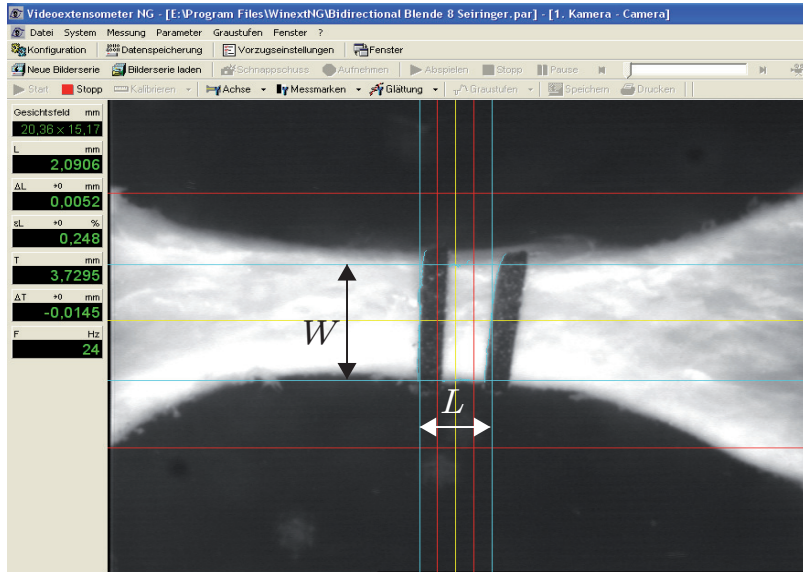
Figure 2.13: Representative screenshot of the videoextensometer before the rupture test
(starting position). The initial length L and width W of the tissue in the un-
loaded configuration is illustrated. L represents the measured gauge length
between the two black markers.
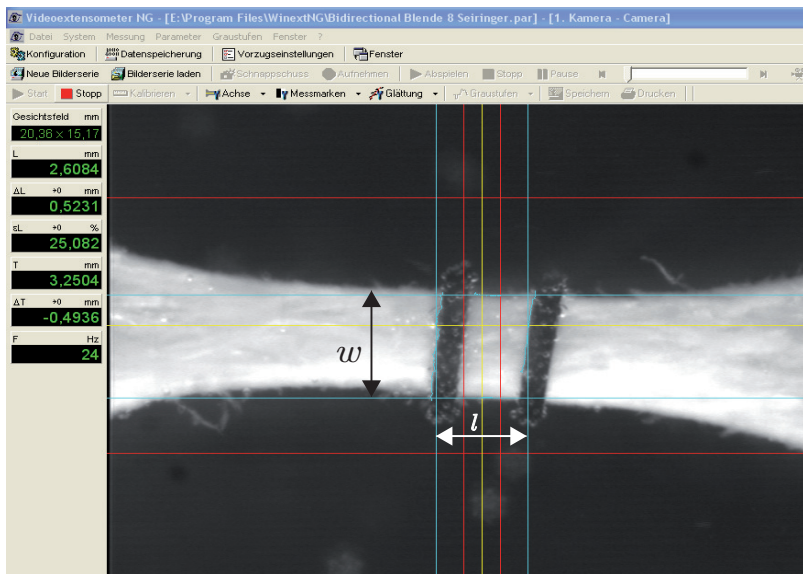
Figure 2.14: Representative screenshot of the videoextensometer during the rupture test.
The actual length l an width w of the tissue in the loaded configuration are
illustrated. l represents the measured gauge lengths between the two black
markers.
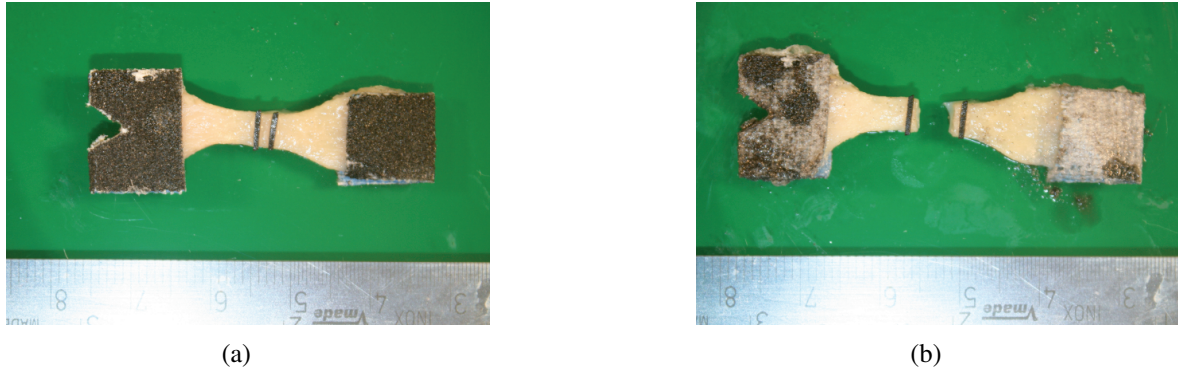
Figure 2.15: Representative photographs of (a) a prepared aortic tissue specimen ready for uniaxial tension test and of (b) an already successfully ruptured specimen. In (a) the markers for rupture measurement of the axial deformation can be seen.

2.7 Shear tests

2.7.1 Theoretical background

This section describes how the shear properties of the aortic tissues are determined by performing triaxial shear tests (mode *II* tests). With the assumption of the mechanical properties of orthotropic soft tissue, there are six possible modes of simple shear defined (Dokos et al., 2002) .

The in-plane shear properties of the $z\theta$-plane can be seen in panel (b) of Fig. 2.16. These tests make it possible to determine the ultimate shear strength values τ_{rz}^u in the axial direction and $\tau_{r\theta}^u$ in the circumferential direction. Panel (c) of Fig. 2.16 shows the out-of-plane shear properties in the $r\theta$-plane. Performing the test in the radial direction results in the ultimate shear strength value τ_{zr}^u and performing the test in the circumferential direction results in the shear strength value $\tau_{z\theta}^u$. Further, out-of-plane shear properties in the rz-plane can be seen in panel (d). Shearing in radial direction results in the shear strength value $\tau_{\theta r}$ and shearing in the axial direction results in the ultimate shear strength value $\tau_{\theta z}^u$.

It is only possible to measure four of the listed above six shear strength values. In theory the shear in the radial direction is cited, but in practice it is not possible because the radial direction is too thin to perform these tests. Therefore, it speaks for itself, that the shear strength values τ_{zr}^u and $\tau_{\theta r}^u$ are not possible to be determined experimentally.
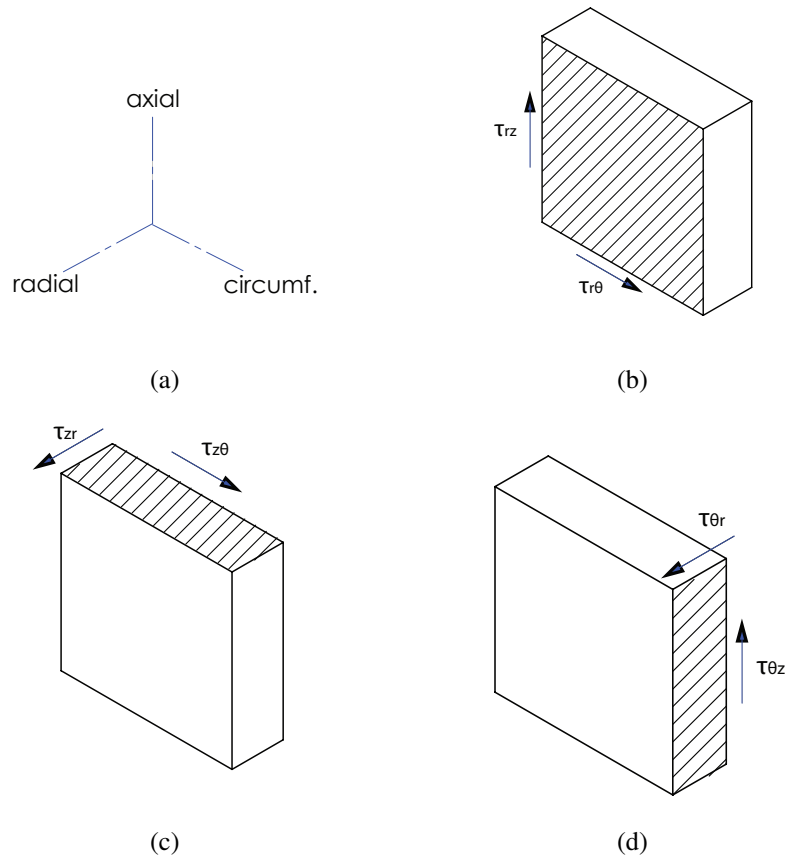
Figure 2.16: Sketches of the six different simple shear properties (modes) defined with respect to the circumferential (θ-axis), axial (z-axis) and radial (r-axis) direction. Arrows on the scotches indicate the shear directions. The first letter denotes the normal vector of the plane that is being sheared. The second letter denotes the direction in which the face is shifted. For example sketch (b) shows the shear in the $z\theta$-plane with shear in the z and in the θ direction, respectively. (c) shows shear in the $r\theta$-plane, and (d) shear in the rz-plane. A labeling of the axes is shown in panel (a)

2.7.2 Specimen preparations

At first, the in-plane shear tests in the $z\theta$-plane were performed. Small rectangular tissue samples with the dimensions of 5mm in length and 4mm in width were prepared from the whole aortic sample. A surgical scalpel and a magnifier were used in order to prepare the specimen as precisely as possible. Afterwards an incision of 1mm depth along the width of the sample was made to induce a breaking point. As a consequence the surface which was sheared was reduced to a square surface of 4mm × 4mm. As already mentioned, two tissue samples were sheared one in axial and one in circumferential direction as shown in Fig. 2.17.

For the out-of-plane shear tests in $r\theta$- and in rz-plane, a special specimen preparation protocol was necessary, because there are no reports available for out-of-plane shear tests in the literature. Different geometries were tested to obtain out-of-plane shear strength. A detailed description of the development for the final setup is described in Sec. 4.4.

The tissue specimen has been prepared with 8mm in length and 3mm in height as shown in Fig. 2.18. The longer side (8mm) is also the direction in which the specimen will be sheared. To induce a predetermined breaking point, incisions were made from both sides starting from the shorter side (3mm) parallel to the shearing direction. Incisions are represented by the dashed lines in Fig. 2.18.
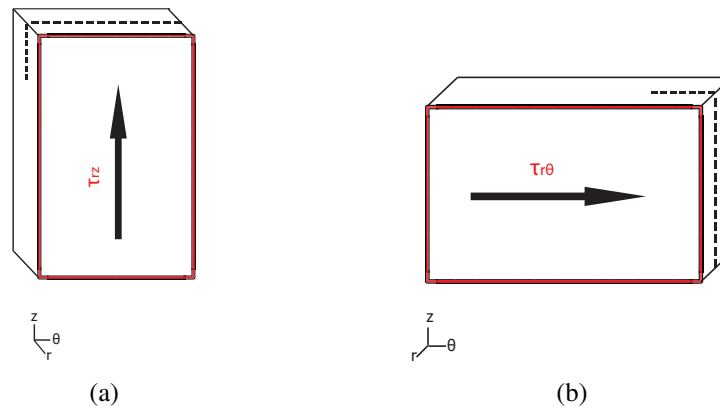
Figure 2.17: Sketch of the in-plane-shear test specimens: The shear properties of the $z\theta$-plane are determined using these specimen geometries. (a) in-plane shear in the axial direction and (b) in-plane shear in the circumferential direction, respectively. Arrows indicate the shear directions. The surfaces are glued on cylindrical stamps for inserting them into the testing setup. In the middle of the shorter edge an incision of 1mm parallel to the shearing direction was made, which is indicated by the dashed line.
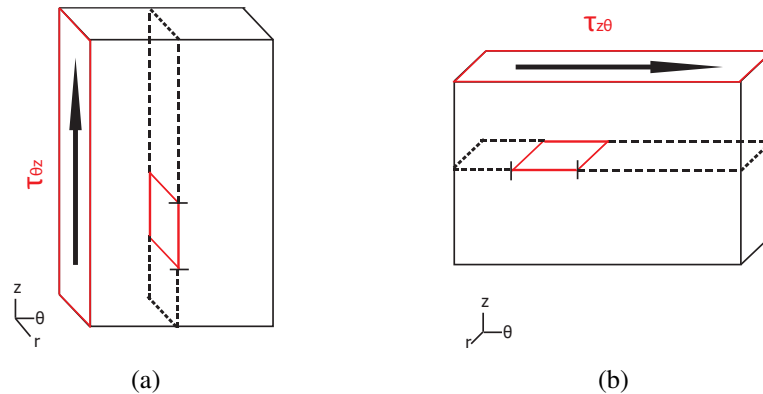
Figure 2.18: Sketch of the out-of-plane shear test specimens: (a) shear properties of the rz-plane and (b) shear properties of the $r\theta$-plane are determined using the shown specimen geometries. Arrows indicate the shear directions. The surfaces are glued on the cylindrical stamps. In the middle of the shorter edge incisions parallel to the shearing direction were made on both sides, which are indicated by the dashed lines. The sheared surface is shown by the red area, between the incised surfaces. It is about 1mm in length, parallel to the longer edge.

2.7.3 Testing Procedure

The specimens were mounted on the triaxial shear testing device between two cylindrical metallic "stamps" used as specimen holders. This specimen fixation was also described in the study by Sommer et al. (2013). Before the procedure both metallic stamps had to be purified from fat by the use of a disinfection agent. The specimen was attached onto the face of the upper cylindrical specimen holder as can be seen in Fig. 2.19. Sandpaper and a thin consistent layer of cyanoacrylate adhesive was used to place the specimen. Sandpaper lead to a better attachment of the sample to the specimen holder and so the rate of successful tests was significantly increased. For the successful tests it was important to not place the super adhesive on any wrong position of the specimen, otherwise the measurements could be falsified. After about three minutes of drying duration for the adhesive both metal stamps were mounted on the machine and the setup was ready for testing.
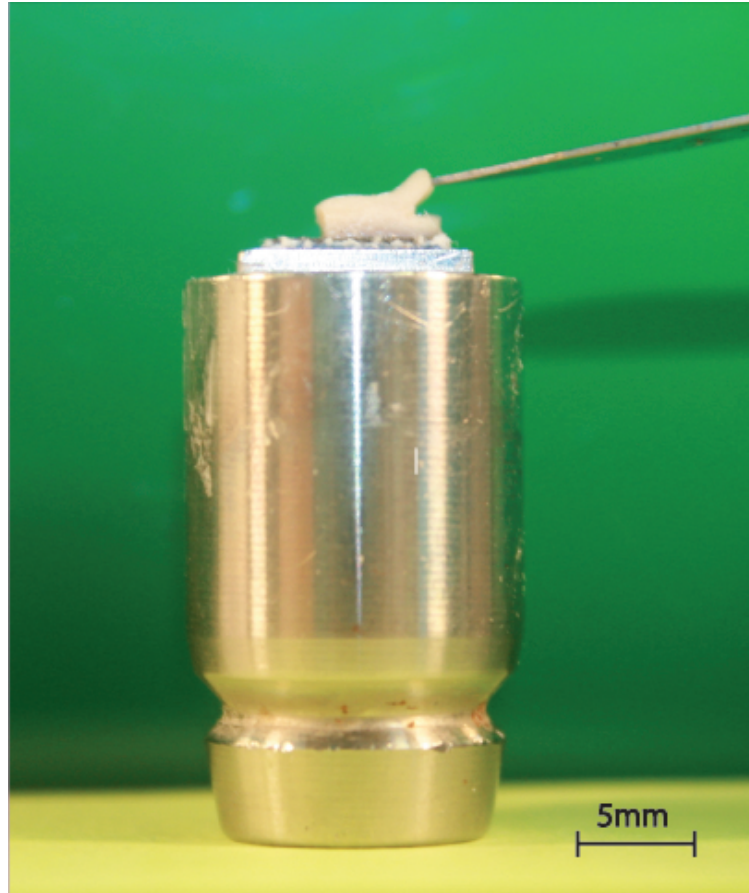
Figure 2.19: Photograph of an aortic tissue specimen attached to the upper specimen holder. Also the cut of 1mm for the in-plane shear tests can be seen.

2.7.4 Testing Protocol

The upper metal part where the specimen was fixed was mounted at the triaxial testing device. Before the testing procedure was started parameters like the exact geometrical dimensions of the medial aortic block, measured using a micrometer, were entered into the "TestXpert II" software. Moreover, several settings such as the moving speed of the x-axis, were defined. The axis labeling was done in reference to the testing machine. In the case of in-plane shear tests in the circumferential direction the x, y and z coordinates of the machine were representative of the tissue directions θ, z and r. Subsequently the software was started which resulted in the lower platform and the upper platform of the machine moving together until a certain distance was reached. Next the super adhesive was placed on the lower metal part. The z-transverse is moved towards the lower platform to adhere the sample onto the lower specimen holder. The tissue was compressed with a force of about 1N for about fife minutes. Meanwhile, the adhesive had enough time to harden, so that the sample could not detach from the fixing stamps. Afterwards the z-axis was moved

back to the tension free state of 0N. In the next step the perspex container was manually filled with PBS solution. The solution had a temperature of 37°C which was maintained by the use of a heating spiral and controlled using a thermometer.

During testing the lower platform moved relative to the fixed upper platform with a constant speed of 1mm/min in the x-direction. In other words, a shearing force was applied to the bottom of the specimen, while the top is held in place. As a result the tissue was exposed to simple shear. Simple shear means that a combination of shear and extension is applied on the specimen which fibers, sheets and ground substance get elongated.

Representative photographs of a tissue specimen during simple shear is shown in Fig. 2.21. The applied force that led to failure is defined as the shear failure force and is measured in Newton. The resulting forces in three axes (x, y, z) were measured. Additionally, shear strain and shear stresses were continuously computed by the software and stored in a *.xls* file which was used for data evaluation.

In the case of simple shear the amount of shear γ is defined as the change in angle between two parallel layers in a material body. It is calculated as the ratio of the relative in-plane displacement of two parallel layers to their separation distance as shown in Eq. (2.7). The shear stress τ (N/mm^2) is the stress acting in a body parallel to the plane, if a force f is acting on the upper edge of a body, see Fig. 2.20. It can be expressed as the shear force f divided by the shear area a as shown in Eq. (2.8).

$$\gamma = \frac{\Delta x}{l} = \tan(\theta) \tag{2.6}$$

γ ...   shear strain   []
Δx ...   shear displacement   [mm]
l ...   seperation distance   [mm]

For tough materials and and small angles a simplification leads to

$$\tan(\theta) \approx \theta \tag{2.7}$$

but this is not valid for smooth biological tissue.

$$\tau = \frac{f}{a} \tag{2.8}$$

τ ...   shear stress   [N/mm^2 = 1MPa]
f ...   force applied   [N]
a ...   cross sectional area   [mm^2]

The shear stress τ is thus the division of the force f and the cross sectional area a and is measured in N/mm^2.
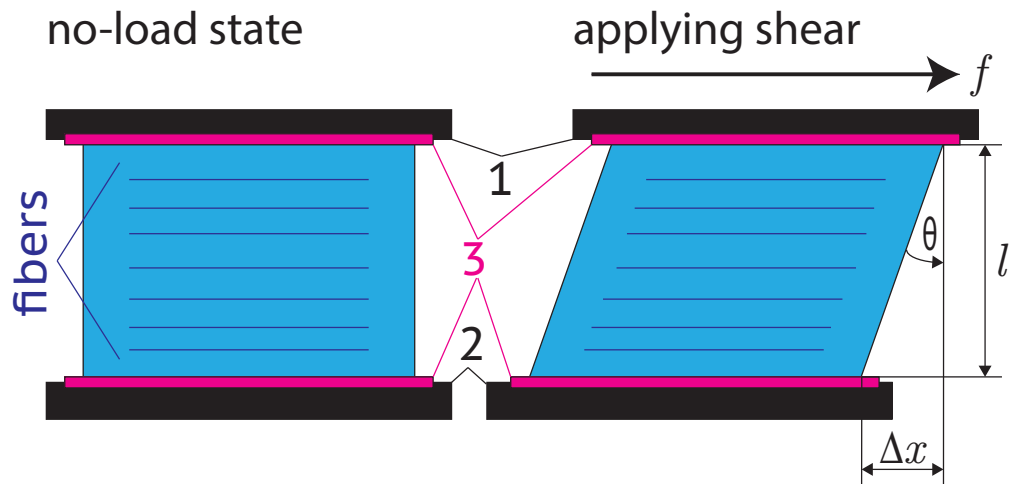
Figure 2.20: Application of simple shear (in-plane mode). The force f acts on the upper surface resulting in an amount of shear γ. Description of the character: 1, moving plates; 2, fixed plates; 3, glue; f, force; l, height of the specimen; θ, shear angle; Δx, sheared distance
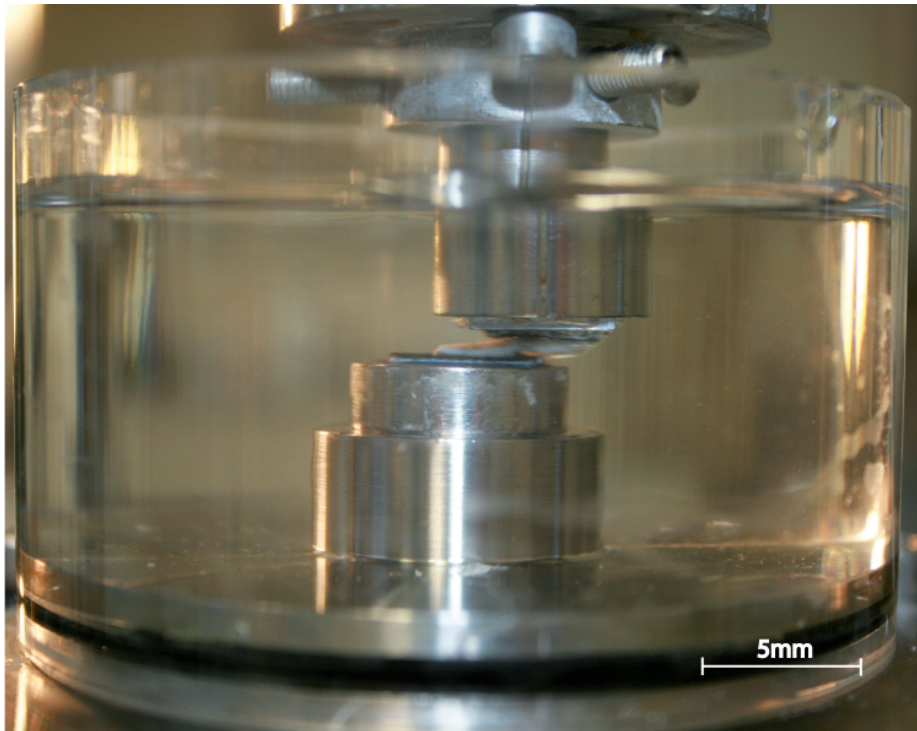
Figure 2.21: Photograph of an aortic tissue specimen, while it is tested under simple shear loading.

3 Results

In this chapter all results of the different conducted rupture tests (uniaxial tension and shear tests), obtained from all individual samples are listed and small interpretations are also given. In total 13 human thoracic aortic tissues was investigated. Each sample was assigned with a different color which was maintained for all plots in this Section. The visualization of the results has been roughly divided into two groups: dissected and aneurysmal aortic tissue specimens, whereby those specimen with tissue malformation, i.e. Mass- or Marfan syndrome are given in a separate plot.

3.1 Direct Tension test

Figures 3.1, 3.2 and 3.3 visualize the calculated Cauchy stress vs. stretch response of the individual direct tension tests. There can be observed an obvious characteristic behavior over all stress-stretch responses of the different direct tension tests. At first the tissue shows an elastic behavior due to increasing displacement which is represented by an ascending steep slope. After an "elastic limit" is reached a second phase of the mechanical tissue response enters, which is strongly nonlinear. Damage softening and micro defects gradually occur. After reaching the maximum of the Cauchy stress vs. stretch response a third phase of mechanical tissue response. The tissue is going to dissect until complete tissue failure. This behavior is characterized by a descending steep slope which merges into a flatter plateau until the course drops to zero. This mechanical behavior during direct tension tests of medial tissue of human abdominal aortas and human carotid bifurcations is also described in the studies by Tong et al. (2011) and Sommer et al. (2008). It is known that the Cauchy stress vs. stretch response curve behaves slightly non-linear within the first section and does only show marginal increasing stiffness at higher strains. It may thus be concluded that in contrast to the axial and circumferential direction the media behaves almost linear elastic in the radial direction.

The results of the ultimate radial failure stresses and their corresponding ultimate stretches are given in Tab. 3.1. In contrast, in Tab. 3.2 the mean values and standard deviations (SD) of the radial failure stresses and stretches of the different samples categorized according to their disease are given.

Table 3.1: Measured ultimate radial failure stresses, corresponding stretches of the different samples, and the corresponding color in the Cauchy stress vs. stretch diagram. (σ^u, ultimate radial failures stress; λ^u, corresponding ultimate stretch)

Specimen	σ^u	λ^u	color
	[kPa]		in diagram
*III*a	97	3.52	light-blue
*III*b	136	2.00	blue
IV	84	1.91	green
V	73	1.59	orange
VI	199	2.52	purple
VII	77	2.61	cyan
VIII	87	1.87	yellow
IX	233	2.72	red
X	106	2.05	brown
XI	138	3.61	magenta
XII	167	2.16	light-green
XIII	273	2.08	black
mean	139	2.45	
± SD	± 63	± 0.65	

Table 3.2: Mean values and corresponding standard deviations (SD) of the radial failure stresses and stretches of the different samples categorized according to their disease. ($\overline{\sigma}_{rr}^u$, average radial failures stress; $\overline{\lambda}^u$, corresponding ultimate stretch)

Disease	$\overline{\sigma}^u$	$\overline{\lambda}^u$
	[kPa]	
dissected	111 ± 27	2.8 ± 0.9
aneurysmatic	172 ± 73	2.2 ± 0.4
aneurysmatic (tissue disorders)	104 ± 21	2.5 ± 0.6
mean ± SD	139 ± 63	2.4 ± 0.6
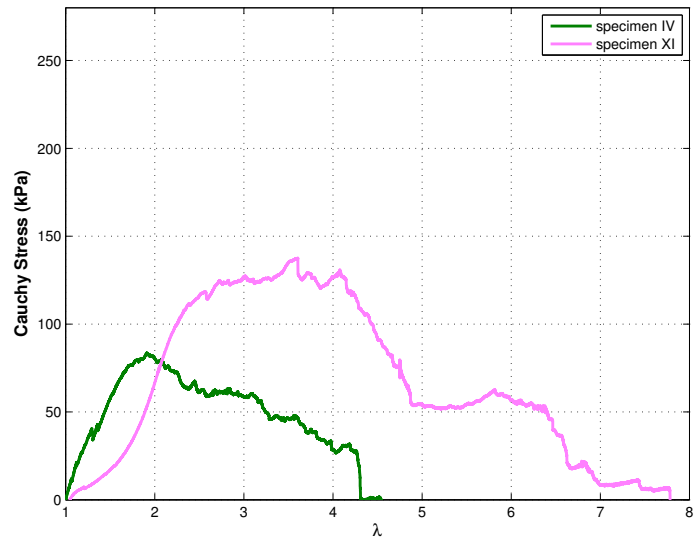
Figure 3.1: Cauchy stress vs. stretch response of all dissected specimens during direct tension tests of the media.
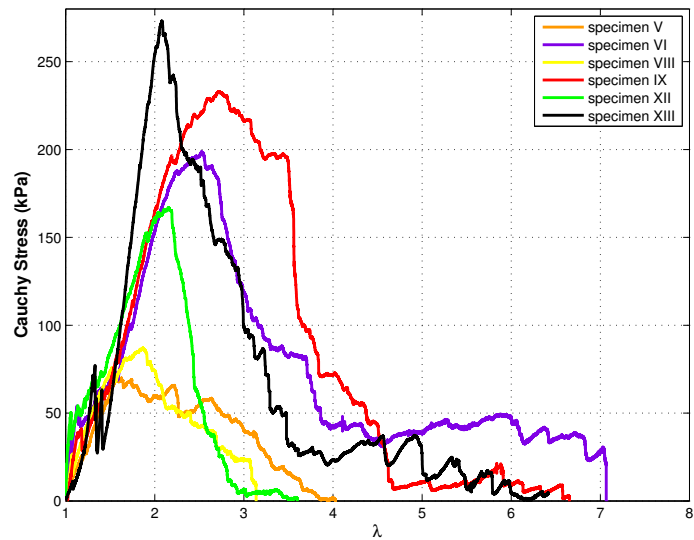
Figure 3.2: Cauchy stress vs. stretch response of all aneurysmatic specimens during direct tension tests of the media.
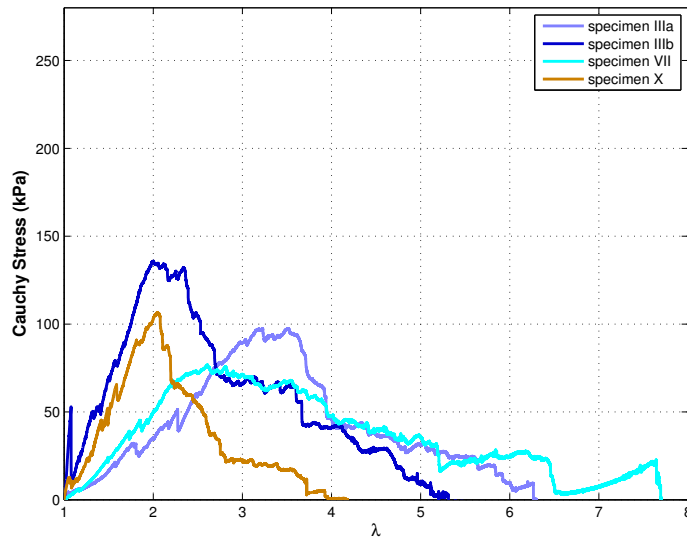
Figure 3.3: Cauchy stress vs. stretch response of all aneurysmatic specimen with tissue disorder during direct tension tests of the media.

3.2 Uniaxial tension test

In Tab. 3.3 the measured ultimate tension stresses and corresponding stretches of the tested samples obtained from two separate orientations that fractured within the gauge region are summarized. Missing values indicate either that the performed test was not available or not successful. In Tab. 3.4 the mean values and standard deviations (SD) of the ultimate tension stresses and ultimate stretches of the different samples categorized according to their disease are given.

Figures 3.4, 3.6 and 3.8 show the mechanical response of the uniaxial tension tests in axial direction, while in Figs. 3.5, 3.7 and 3.9 the results in the circumferential direction of all samples subdivided into their respective diseases (dissected, aneurysmatic and aneurysmatic with tissue disorder) are shown. A comparison of the mechanical response between the axial and circumferential direction such as for example in Figs. 3.4 and 3.5 remarkably show that stress values at fracture for the circumferential direction are much higher than those in the axial direction. This behavior is attributed to the anisotropic behavior of the medial tissue.

Table 3.3: Measured ultimate tension stresses, the corresponding ultimate stretches and the associated color in the tension stress vs. stretch diagram of samples that fractured in the gauge region. ($\sigma_{\theta\theta}^u$, ultimate tension stress in the circumferential direction; σ_{zz}^u, ultimate tension stress in the axial direction; $\lambda_{\theta\theta}^u$, ultimate stretch in the circumferential direction; λ_{zz}^u, ultimate stretch in the axial direction)

Specimen	$\sigma_{\theta\theta}^u$ [kPa]	$\lambda_{\theta\theta}^u$	σ_{zz}^u [kPa]	λ_{zz}^u	color in diagram
II	490	1.50	357	1.47	gray
IIIa	815	1.34	335	1.57	light-blue
V	976	1.68	260	1.87	orange
VI	1379	1.39	792	1.66	purple
VII	525	1.36	443	1.59	cyan
IX	1042	1.59	759	1.55	red
XI	400	1.65	261	1.49	magenta
XII	1411	1.55	506	1.81	light-green
XIII	1480	1.63	671	1.74	black
mean	947	1.52	487	1.64	
± SD	± 394	± 0.12	± 196	± 0.14	

Table 3.4: Mean values and SD of the ultimate tension stresses and ultimate stretches of the different samples, categorized according to their disease. ($\overline{\sigma}_{\theta\theta}^u$, average ultimate tension stress in the circumferential direction; $\overline{\sigma}^u$, average ultimate tension stress in the axial direction; $\overline{\lambda}_{\theta\theta}^u$, average ultimate stretch in the circumferential direction; $\overline{\lambda}_{zz}^u$, average ultimate stretch in the axial direction)

Disease	$\overline{\sigma}_{\theta\theta}^u$ [kPa]	$\overline{\lambda}_{\theta\theta}^u$	$\overline{\sigma}_{zz}^u$ [kPa]	$\overline{\lambda}_{zz}^u$
dissected	444 ± 45	1.57 ± 0.07	309 ± 48	1.48 ± 0.00
aneurysmatic	1258 ± 207	1.57 ± 0.10	597 ± 196	1.73 ± 0.11
aneurysmatic (tissue disorder)	670 ± 145	1.35 ± 0.01	389 ± 54	1.58 ± 0.01
mean ± SD	947 ± 394	1.52 ± 0.12	487 ± 196	1.64 ± 0.14
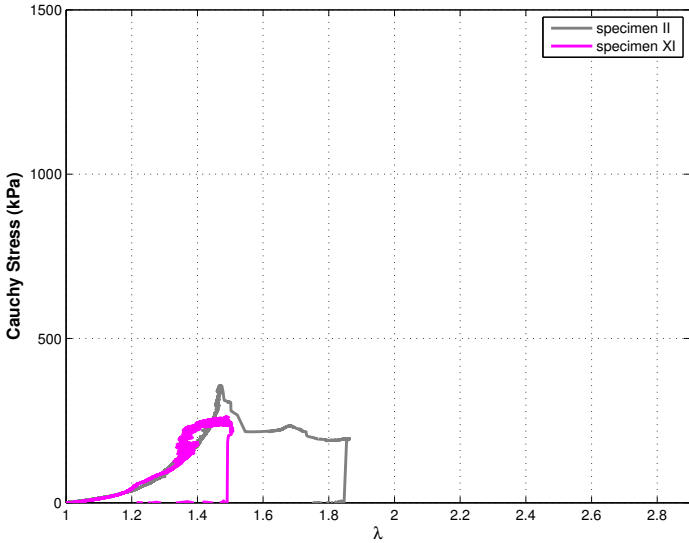
Figure 3.4: Uniaxial tension Cauchy stress vs. stretch behavior of all dissected specimens in the longitudinal direction.
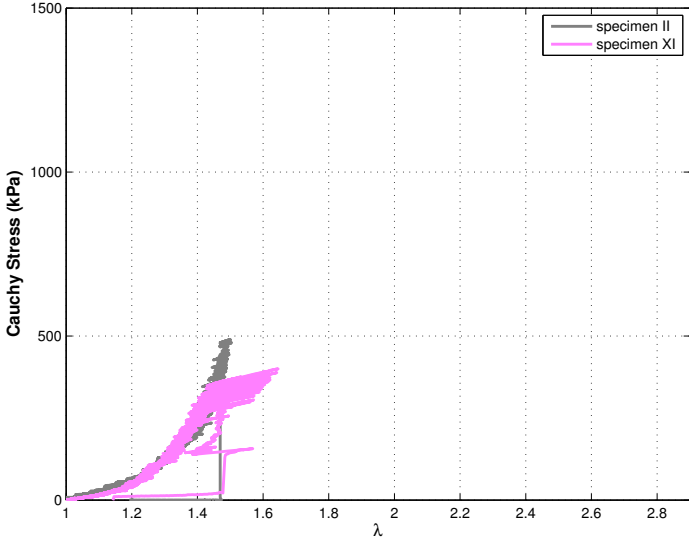
Figure 3.5: Uniaxial tension Cauchy stress vs. stretch behavior of all dissected specimens in the circumferential direction.
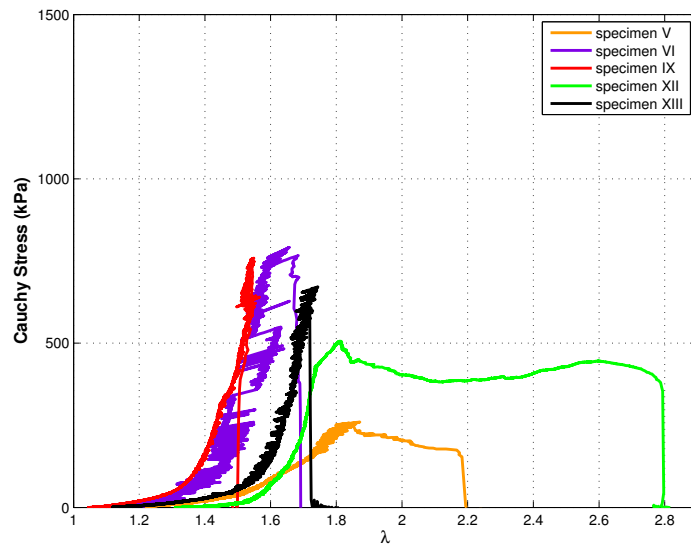
Figure 3.6: Uniaxial tension Cauchy stress vs. stretch behavior of all aneurysm specimens in the longitudinal direction.
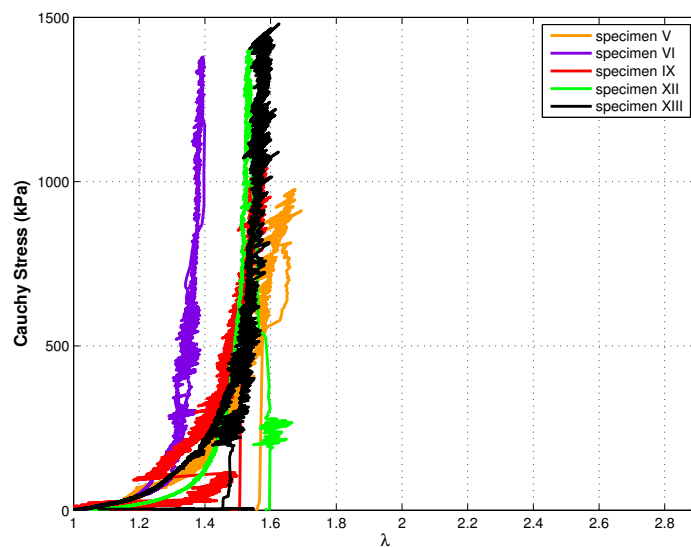
Figure 3.7: Uniaxial tension Cauchy stress vs. stretch behavior of all aneurysm specimens in the circumferential direction.
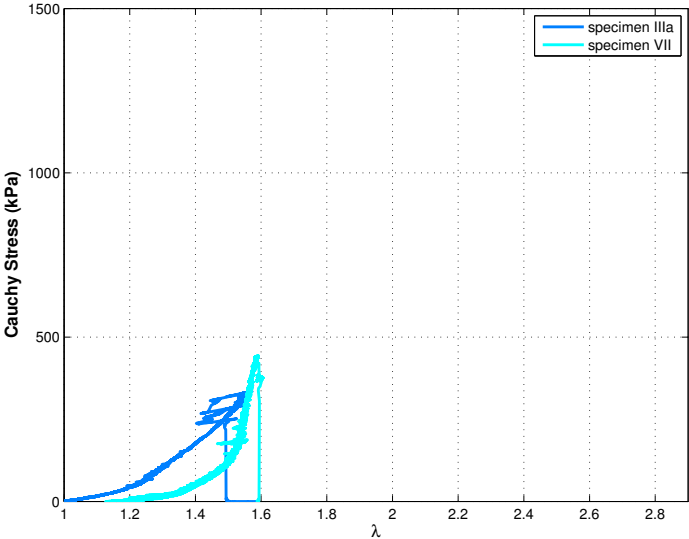
Figure 3.8: Uniaxial tension Cauchy stress vs. stretch behavior of all aneurysm specimens with tissue disorders in the longitudinal direction.
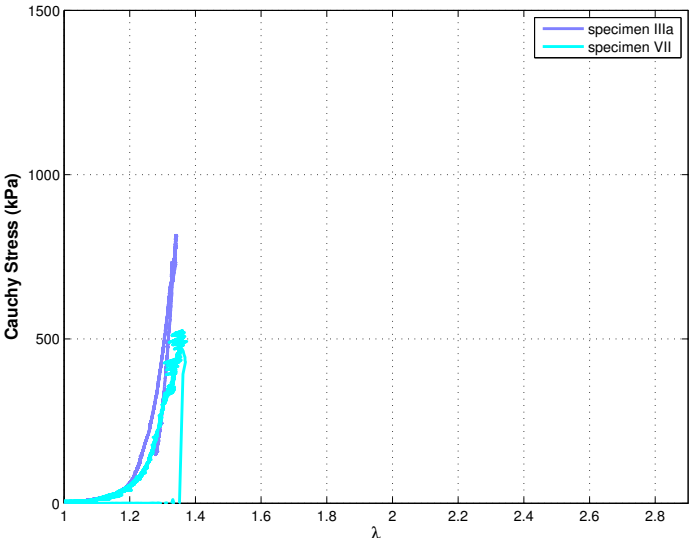
Figure 3.9: Uniaxial tension Cauchy stress vs. stretch behavior of all aneurysm specimens with tissue disorders in the circumferential direction.

3.3 Shear test

3.3.1 In-plane shear test

Figures 3.10, 3.12 and 3.14 show the results of the in-plane shear tests in longitudinal direction z, whereas Figs. 3.11, 3.13 and 3.15 show the results of the in-plane shear tests in the circumferential direction θ of all samples subdivided into their diseases (dissected, aneurysmatic and aneurysmatic with tissue disorders).
All tested specimens show on average the same mechanical characteristic. With increasing shear stresses the aortic tissue behaves nonlinear in each direction and shows marginal anisotropic shear properties.

   The aim of this test was to determine the shear failure stresses of the tissue. This value is given by the maximum shear stress value of each curve. After reaching this point where the crack is initiated the tissue and especially the medial layer began to tear until it is fully dissected. In view of this fact, the further course of the curve is no longer meaningful, because the crack propagation was always deviated from the shear plane. For analysis, the data are only useful up to the maximum stress value of the curves, because the further data can not be defined by the controlled simple shear. The ultimate shear strength values in both directions are close to each other. It should be mentioned that the longitudinal direction z shows stiffer shear behavior than the circumferential direction θ during shearing in the rz- and $r\theta$-modes.

Table 3.5: Measured ultimate shear failure stress of the in-plane shear tests, obtained from the different samples from two separate orientations, and corresponding color in the cauchy shear stress vs. shear displacement diagram. ($\tau_{r\theta}^u$, ultimate shear strength in the circumferential direction; τ_{rz}^u, ultimate shear strength in the axial direction; $\gamma_{r\theta}^u$, ultimate shear strain in the circumferential direction; γ_{rz}^u, ultimate shear strain in the axial direction)

Specimen	$\tau_{r\theta}^u$ [kPa]	$\gamma_{r\theta}^u$	τ_{rz}^u [kPa]	γ_{rz}^u	color in diagram
I	107	1.45	122	2.42	peach
II	93	0.98	126	1.13	gray
*III*a	56	1.96	88	1.08	light-blue
*III*b	74	0.65	102	1.40	blue
IV	93	0.96	118	1.52	green
V	57	1.54	92	1.30	orange
VI	120	1.97	135	1.98	purple
VII	58	1.76	92	1.69	cyan
VIII	77	1.43	118	1.65	yellow
IX	153	1.89	185	1.74	red
X	76	1.85	103	1.35	brown
XI	91	1.27	111	1.74	magenta
XII	74	1.63	100	2.12	light-green
XIII	100	1.63	165	2.13	black
mean	88	1.50	118	1.66	
± SD	± 26	± 0.39	± 27	± 0.38	

Table 3.6: Comparison of the average ultimate shear failure stresses of the in-plane shear stress-strain relationship, categorized according to their disease. ($\tau_{r\theta}^u$, Ultimate shear strength in the circumferential direction; τ_{rz}^u, Ultimate shear strength in the axial direction)

Disease	$\overline{\tau}_{r\theta}^u$ [kPa]	$\overline{\gamma}_{r\theta}^u$	$\overline{\tau}_{rz}^u$ [kPa]	$\overline{\gamma}_{rz}^u$
dissected	96 ± 6	1.16 ± 0.20	118 ± 6	1.70 ± 0.47
aneurysmatic	97 ± 32	1.68 ± 0.19	133 ± 34	1.82 ± 0.29
aneurysmatic (tissue disorder)	66 ± 9	1.56 ± 0.53	96 ± 6	1.38 ± 0.22
mean ±SD	88 ± 26	1.50 ± 0.39	118 ± 27	1.66 ± 0.38
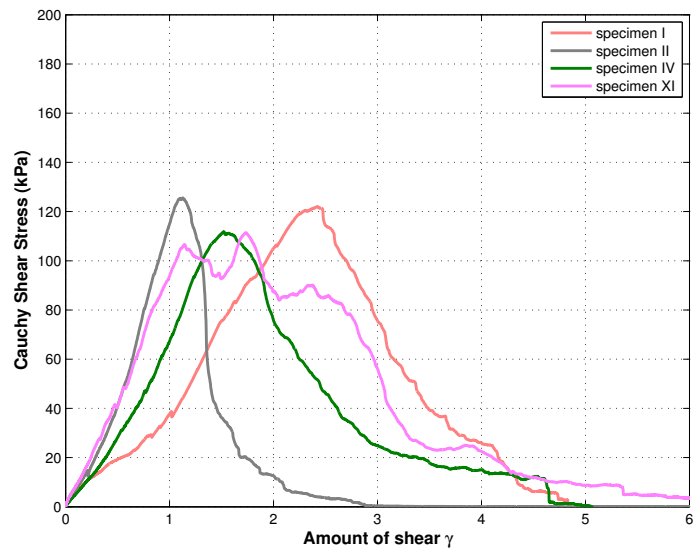
Figure 3.10: Cauchy shear stress vs. amount of shear relationship of all dissected specimens of in-plane-shear tests in the rz-mode.
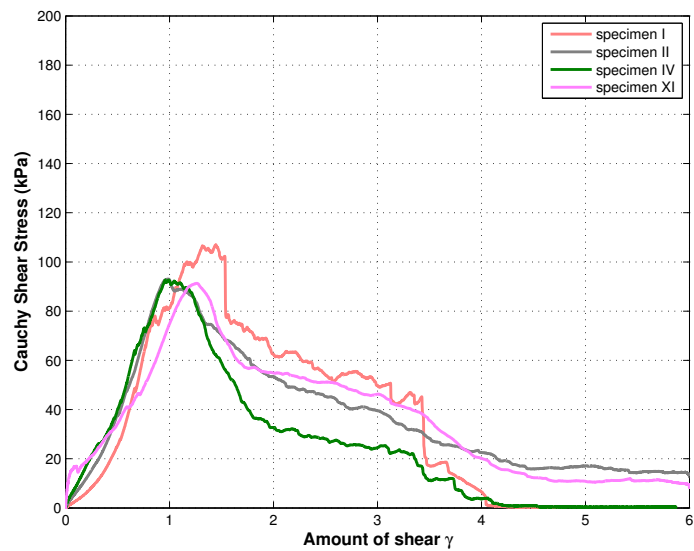
Figure 3.11: Cauchy shear stress vs. amount of shear relationship of all dissected specimens of in-plane-shear tests in the $r\theta$-mode.
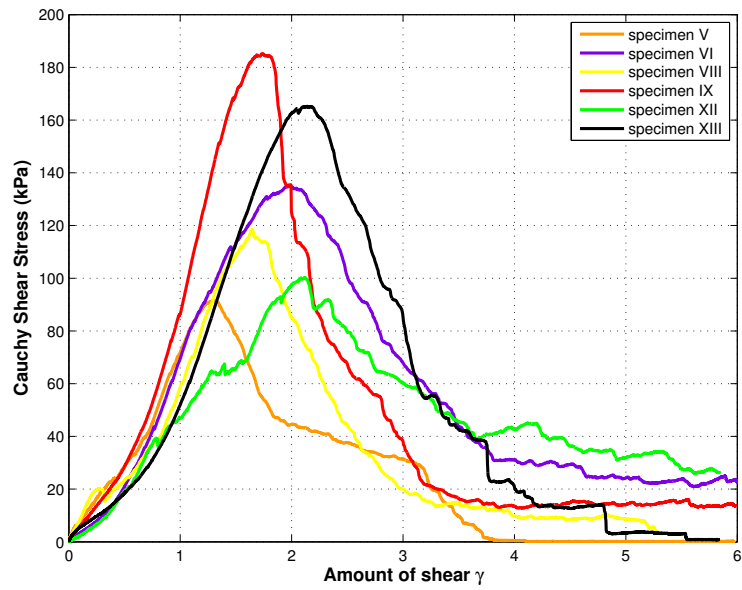
Figure 3.12: Cauchy shear stress vs. amount of shear relationship of all aneurysm speci-
          mens of in-plane-shear tests in the rz-mode.
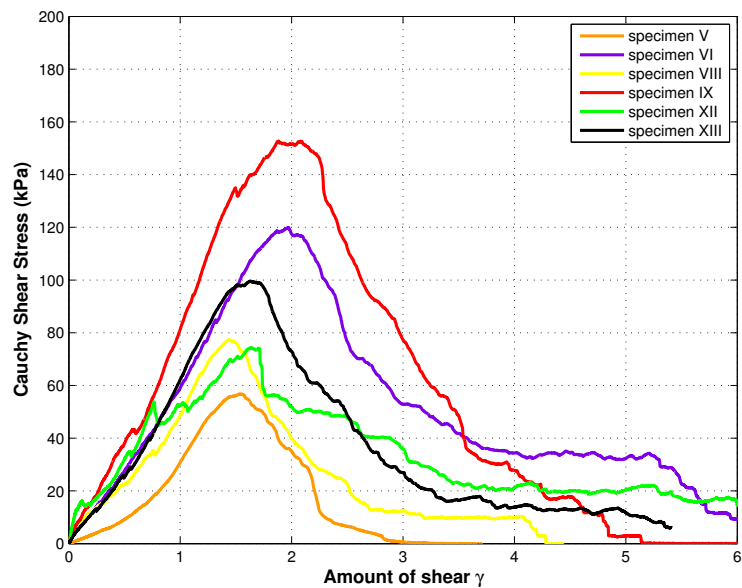
Figure 3.13: Cauchy shear stress vs. amount of shear relationship of all aneurysm speci-
          mens of in-plane-shear tests in the $r\theta$-mode.
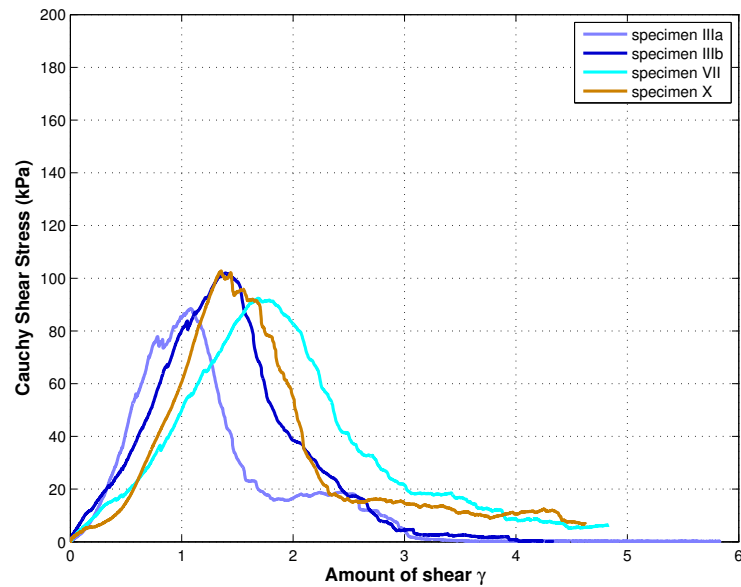
Figure 3.14: Cauchy shear stress vs. amount of shear relationship of all aneurysm specimens with tissue disorder of in-plane-shear tests in the rz-mode.
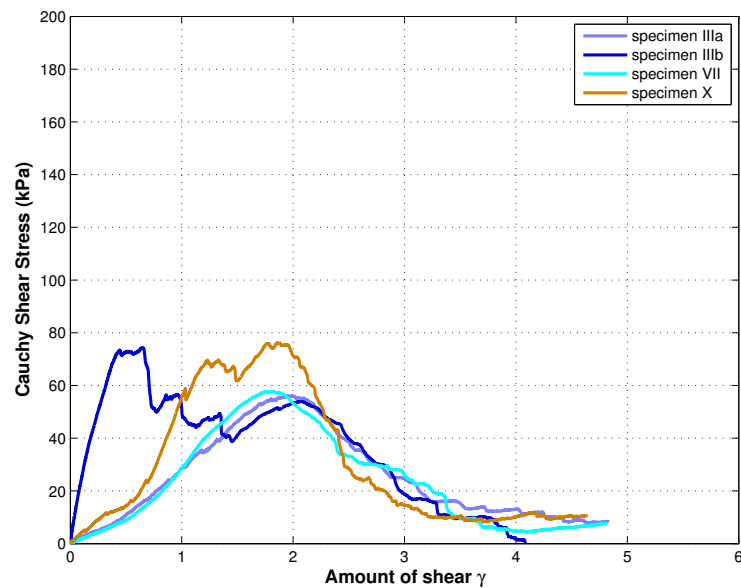
Figure 3.15: Cauchy shear stress vs. amount of shear relationship of all aneurysm specimens with tissue disorder of in-plane-shear tests in the $r\theta$-mode.

3.3.2 Out-of-plane shear test

Figures 3.16, 3.18 and 3.20 show the results of the out-of-plane shear tests in longitudinal direction z, whereas Figs. 3.17, 3.19 and 3.21 show the results of the out-of-plane tests in the circumferential direction θ of all samples subdivided into their diseases (dissected, aneurysmatic and aneurysmatic with tissue disorders).

As also for the in-plane mode, the longitudinal direction z shows stiffer shear behavior than the circumferential direction θ during shearing in the θz- and $z\theta$-modes. Basically, they depict the same mechanical response as the in-plane shear tests. But in comparison with the in-plane shear tests it can be observed that the out-of-plane shear tests exhibit much higher ultimate shear strength values. Consequently, it can be said that the material is much stiffer in the out-of-plane direction than in the in-plane direction.

In Tab. 3.7 all ultimate shear strength values of the individual out-of-plane shear tests are listed, as well as their mean values, which are discussed more more detail in Sec. 4.4. Table 3.6 compares the experimentally obtained data concerning the mean absolute value of the out-of-plane shear tests, divided into the underlying diseases of the respective samples.

Table 3.7: Measured ultimate shear failure stresses of the out-of-plane shear tests obtained from the different samples from two separate orientations, corresponding color in the Cauchy shear stress vs. shear displacement diagram. ($\tau_{z\theta}^u$, ultimate shear strength in the circumferential direction; $\tau_{\theta z}^u$, ultimate shear strength in the axial direction; $\gamma_{z\theta}^u$, ultimate shear strain in the circumferential direction; $\gamma_{\theta z}^u$, ultimate shear strain in the axial direction)

Specimen	$\tau_{z\theta}^u$ [kPa]	$\gamma_{z\theta}^u$	$\tau_{\theta z}^u$ [kPa]	$\gamma_{\theta z}^u$	color in diagram
*III*a	475	0.81	836	0.92	light-blue
V	325	1.97	716	1.68	orange
VI	819	0.94	1375	0.80	purple
VII	629	1.00	1135	1.45	cyan
VIII	716	1.68	1349	1.14	yellow
IX	1233	1.44	2548	1.02	red
X	859	0.84	1037	1.90	brown
XI	814	0.87	1297	1.00	magenta
XII	683	0.76	1138	1.08	light-green
XIII	947	1.23	1292	1.26	black
mean	750	1.06	1272	1.22	
$\pm$SD	$\pm$239	$\pm$0.29	$\pm$473	$\pm$0.33	

Table 3.8: Comparison of the average ultimate shear failure stresses of the out-of-plane shear stress-strain relationship categorized according to their disease. ($\tau_{z\theta}^u$, Ultimate shear strength in the circumferential direction; $\tau_{\theta z}^u$, Ultimate shear strength in the axial direction)

Disease	$\overline{\tau}_{z\theta}^u$ [kPa]	$\overline{\gamma}_{z\theta}^u$	$\overline{\tau}_{\theta z}^u$ [kPa]	$\overline{\gamma}_{\theta z}^u$
dissected	813	0.87	1297	1.01
aneurysmatic	776 ± 281	1.19 ± 0.30	1403 ± 558	1.16 ± 0.27
aneurysmatic (tissue disorders)	654 ± 158	0.88 ± 0.08	1003 ± 124	1.42 ± 0.40
mean $\pm$SD	750 ± 239	1.06 ± 0.29	1272 ± 473	1.22 ± 0.33
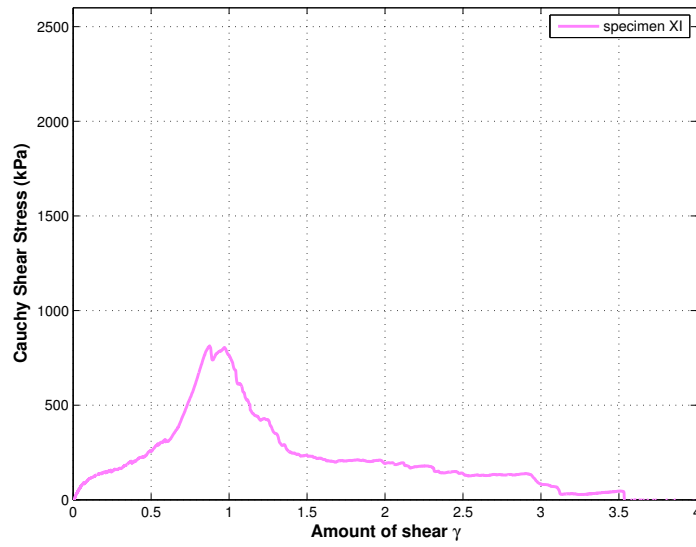
Figure 3.16: Cauchy shear stress vs. amount of shear relationship of all dissected speci-
mens of out of-plane-shear tests in the $z\theta$-mode.
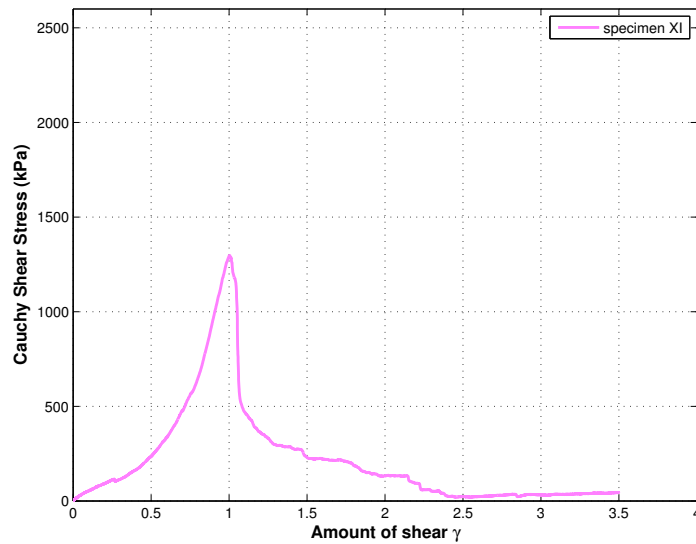
Figure 3.17: Cauchy shear stress vs. amount of shear relationship of all dissected speci-
mens of out of-plane-shear tests in the θz-mode.
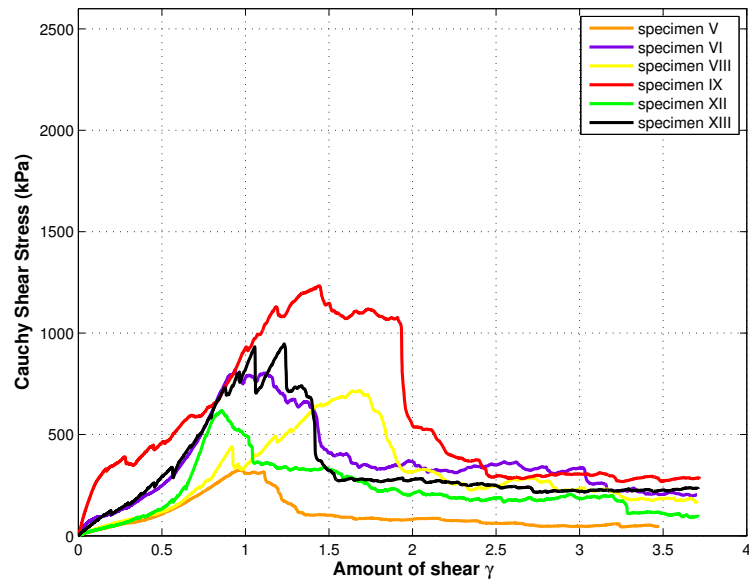
Figure 3.18: Cauchy shear stress vs. amount of shear relationship of all aneurysm speci-
mens of out of-plane-shear tests in the $z\theta$-mode.
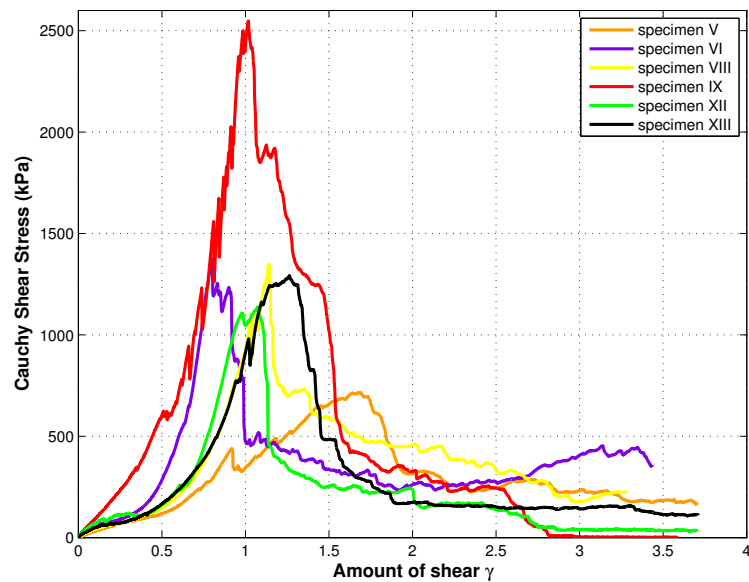
Figure 3.19: Cauchy shear stress vs. amount of shear relationship of all aneurysm speci-
mens of out of-plane-shear tests in the θz-mode.
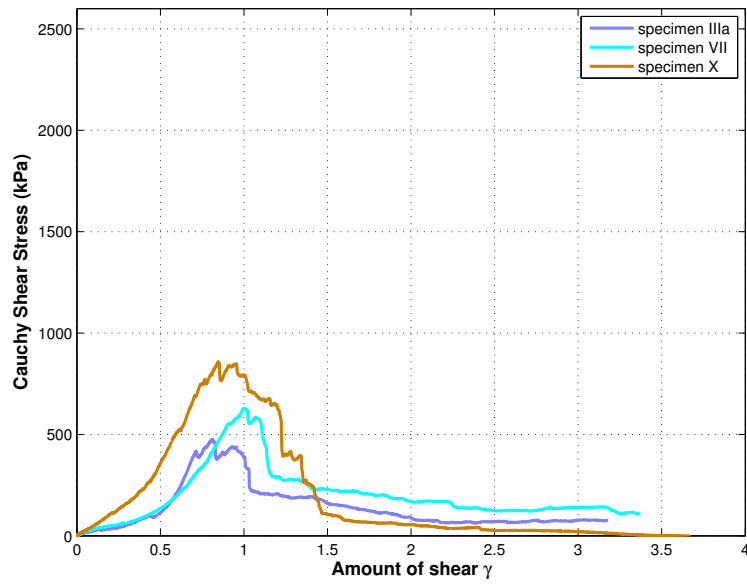
Figure 3.20: Cauchy shear stress vs. amount of shear relationship of all aneurysm speci-
mens with tissue disorder of out of-plane-shear tests in the $z\theta$-mode.
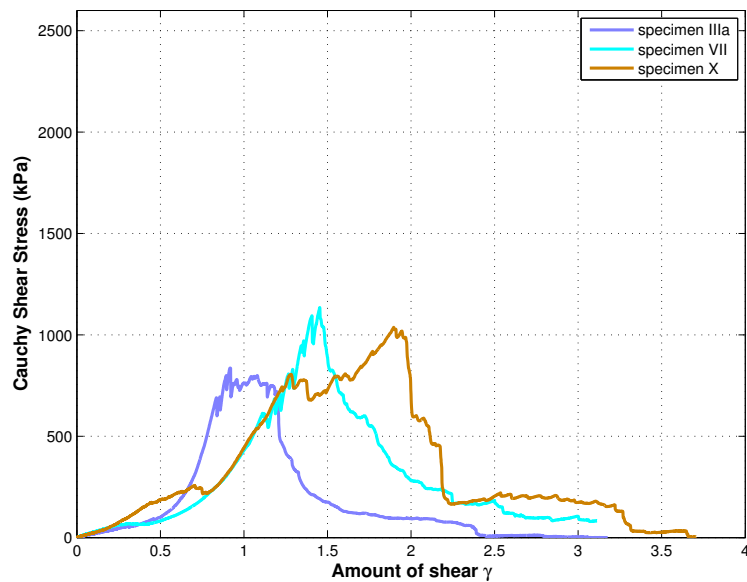
Figure 3.21: Cauchy shear stress vs. amount of shear relationship of all aneurysm speci-
mens with tissue disorder of out of-plane-shear tests in the θz-mode.

4 Discussion

This chapter covers the analysis and discussion of the results obtained in Sec. 3 and a comparison of the observed mechanical behavior of thoracic aortic tissues to other works in the literature. Additionally, circumstances that influenced the measuring process as well as limitations and testing errors are discussed.

4.1 General Aspects

The aim of the study was to determine the mechanical strength of dissected and aneurysmatic thoracic aortic tissues with respect to its anisotropic structure. To our knowledge, this is the first investigation of characterizing the mechanical properties of human thoracic aortic tissues under combined uniaxial tension and simple shear loadings. It is absolutely necessary to receive relevant data of human thoracic aortas for example to adapt the design of aortic stent grafts more realistically. The findings may be an important step forward for assessment and development of a failure criterion for thoracic aortic tissues. In the future, these strength values are indented to serve as input parameters for a failure criterion for thoracic aortas prone to dissection.

This work reports the outcome of experiments related to the mechanical behavior of total of 13 human thoracic aortas. Due to the small specimen size it was not always possible to conduct all tests on every specimen.
Furthermore, tissues with too strong pronounced inhomogeneities like atherosclerotic plaques were unsuitable for this investigation, resulting in loss of tissue and in a reduced specimen number. Upon completion of the individual tests each sample was inspected in order to exclude errors of the measured results caused by penetration of glue along its unattached sides. If that was the case the results were not used.
Especially in the case of biomechanical testing the interpretability of the results depends largely on the environmental conditions, external influences and the accuracy of working. In this context it is also worth to mention that there is a strong correlation between the mechanical properties of arteries and the patient's anamnesis (Hickler, 1990).
In summary one can say that the results of the individual tests showed the overall characteristics of thoracic aortic tissue. Closer investigation of the results of the direct tension, uniaxial tension and triaxial shear tests are stated in a detailed explanation below.

4.2 Direct tension test

In relation to the course of the results of the direct tension test, which is described in section 3.1, the dissection of the media may be characterized.

All direct tension tests were conducted with an extension rate of 1.0 mm/min, but it is not established that this value corresponds to a physiological value. There are no mechanical or clinical data available at which speed a dissection propagates in the case of an *in vivo* situation. It is possible that the dissection properties depend on the rate.

As given in Tab. 3.2 the results of direct tension tests show an average radial failure stress of $\overline{\sigma}_{rr}^{u}$ = *139 ± 63 kPa (mean ± SD, n=11)*. In comparison, the results of rupture tests in axial and circumferential directions as given in Tab. 3.4 report average ultimate tension strengths of $\overline{\sigma}_{zz}^{u}$ = *487 ± 196 kPa* and $\overline{\sigma}_{\theta\theta}^{u}$ = *947 ± 394 kPa* (longitudinal and circumferential direction). It can be hypothesized that the medial tissue is much weaker in the radial direction than in the axial and circumferential directions, which is due to its laminar structure.

Comparison with existing data
The average radial failure stress of the media of $\overline{\sigma}_{rr}^{u}$ = *139 ± 63 kPa (mean ± SD, n=11)* is slightly higher than that of human carotid bifurcations, i.e., 124 ± 25 kPa (mean ± SD, $n=25$), see Tong et al. (2011). A study by Sommer et al. (2008) on human abdominal aortic media reports an average radial failure stress of 140.1 ± 15.9 kPa (mean ± SD, $n=8$), which are similar to the values determined in our experiments on human thoracic aortas. This match is a hint that the results are very realistic and represent the current situation. A study on porcine thoracic aortas by MacLean et al. (1999) shows failure stress values of 61.4 ± 4.3 kPa (mean ± SD, n=7). The comparatively small value may be explained by species differences and high variances.

4.3 Uniaxial tension test

According to Tab. 3.4, the strip samples of the media show on average stress at fracture of $\overline{\sigma}_{\theta\theta}^{u}$ = *947 ± 394 kPa (mean ± SD, n=9)* in the circumferential direction and $\overline{\sigma}_{zz}^{u}$ = *487 ± 196 kPa (mean ± SD, n=9)* in the longitudinal direction. The men values are significant different, which is given by the p-value of the Student's t-test ($p=0.002$). There are about two times higher ultimate tension stresses of the sample oriented in the circumferential direction than those in the longitudinal direction, which reflects a clearly pronounced anisotropic behavior. As can be seen, for example, in Figs. 3.6 and 3.7 the tissue tends to be weaker in the axial direction than in the circumferential direction. The occurring anisotropy is caused by the orientation of the embedded collagen fibers, which are mostly orientated in the circumferential direction, as mentioned in Sec. 1.2.

The mean values for the Cauchy stress-stretch response at the related damage evolution are also listed in Tab. 3.4. The circumferential specimens of the media stiffen at lower applied stretches in comparison to longitudinal specimens, see for example Fig. 3.4 and

Fig. 3.5. In Tab. 3.4 an average ultimate stretch of $\overline{\lambda}^u_{\theta\theta}$ = *1.52 ± 0.12 (mean ± SD, n=9)* in the circumferential direction and an average ultimate stretch of $\overline{\lambda}^u_{zz}$ = *1.64 ± 0.14 (mean ± SD, n=9)* in the longitudinal direction are shown. The men values are not significant different (p=0.054). Stiffness means the ratio of the Cauchy stress to the associated stretch (extension rate). This means that a large slope indicates high stiffness, whereas a smaller slope indicates less stiffness. The results agree with the alignment of the main fibers direction in the medial layer and the findings reported by Weisbecker et al. (2012) of layer-specific damage experiments on human thoracic and abdominal aortas with non-atherosclerotic intimal thickening.

All investigated tissue samples subjected to tension loading show a highly nonlinear and anisotropic behavior. This behavior was also reported for aortic fibrous caps in the studies by Lendon et al. (1993) and Loree et al. (1994).

Comparison with existing data

The study by Schriefl et al. (2012) suggests that the collagen fibers in the media are mainly arranged in the circumferential direction. Results of Holzapfel et al. (2004) on the mechanical response of human iliac arteries during uniaxial tension tests can be explained with this, where the media shows a higher stiffness in the circumferential direction. These findings correlate well with the present results of human thoracic aortas.

The results of similar experiments on strip samples of medial tissue of human coronary arteries with nonatherosclerotic intimal thickening in a study by Holzapfel et al. (2005) show values of 446 ± 194 kPa (mean ± SD, n=9) in the circumferential direction and 419 ± 188 kPa (mean ± SD, n=7) in the longitudinal direction. This values agree with the current study with respect to the circumferential direction, but not with those in the longitudinal direction.

Mohan and Melvin (1982) performed uniaxial tension experiments on strip samples of human descending mid-thoracic aortas to determine the effect of direction of the tissue. The results show ultimate stress values of 172 ± 89 kPa (mean ± SD, n=18) in the circumferential and 147 ± 91 kPa (mean ± SD, n=18) in the longitudinal direction. Higher ultimate stress values in the circumferential direction than in the longitudinal direction are also given in the current study. The results of Mohan and Melvin (1982) also show ultimate stretches of 1.53 ± 0.28 (mean ± SD, n=18) in the circumferential and 1.47 ± 0.23 (mean ± SD, n=18) in the longitudinal direction. These results do not match with ours, but in general there are very low differences according the ultimate stretch in the respective directions.

Authors of several studies have shown that diseased arterial tissue behaves stiffer compared to healthy tissue, see Born and Richardson (1990), Holzapfel et al. (2004) and Topoleski et al. (1997). Holzapfel et al. (2004) showed that the nondiseased media shows an average ultimate tension stress of 202 ± 70 kPa (mean ± SD) and 189 ± 111 kPa (mean ± SD) in the circumferential and axial direction, respectively. It is noteworthy that for the diseased fibrotic media average ultimate tension stresses of 1073.6 ± 289.3 kPa (mean ± SD) and 187.4 ± 8.3 kPa (mean ± SD) in the circumferential and axial directions, respec-

tively, are specified. It is apparent that the media shows significant differences for diseased fibrotic media in comparison to the nondiseased media. Which is in contrast with our findings, where diseased tissue was weaker than the healthy one. However, due to the small sample size of healthy tissue in this study herein, it is difficult to make meaningful comparisons with the tested diseased samples.

Testing errors and limitations
A large number of uniaxial tension tests failed because the fracture of the sample occurred near one of the clamps instead in the gauge region. A further limitation of the testing results was due to the slippage of the specimen out of the clamps. If there was enough tissue material available, a second sample was prepared and tested.

In some tests, the curves of measurements were very noisy in the area close to the fracture. If the noise was too large, they are not depicted in the plots. This observation is due to the slight change of marker positions during the tension tests. The camera of the video extensometer varied between different points along the two markers which resulted in the horizontal oscillation of the curves in the plots. As a result the plots had to be fitted with a smoothing algorithm during data evaluation with *MATLAB*. This problem can be seen for example in Fig. 3.7 indicated by the red curve of sample *IX*.

4.4 Shear Test

There are limited data available on simple shear loading of soft biological tissues. Comparable data in which the amount of shear leads to failure of the tissue is not available. One of the few studies was conducted by Dokos et al. (2002) with the topic of shear properties of passive ventricular myocardium.

In general, there was a clear indication of nonlinear and anisotropic mechanical behavior for the medial tissue of the ascending and descending aortas as far as the aortic arch under simple shear which is typical for soft biological tissue. A study of Sommer et al. (2008) coincides with these findings, because adipose tissue was also identified as a nonlinear and anisotropic material using biaxial tension tests and triaxial shear tests.

   Regarding the maximum shear failure stresses of all performed shear tests, all figures in Sec. 3.3 show the anisotropic mechanical behavior of thoracic aortic tissue. On average the performed tests exhibit markedly higher ultimate shear strength values in the longitudinal direction than in the circumferential direction under shear deformation.

In the case of in-plane shear tests, the tissue exhibits average shear rupture stresses of $\overline{\tau}_{r\theta}^{u} = 88 \pm 26$ *kPa (mean $\pm$ SD)* in the circumferential and $\overline{\tau}_{rz}^{u} = 118 \pm 27$ *kPa (mean $\pm$ SD)* in the longitudinal direction, during shearing in the $r\theta$- and rz-modes. The mean values are significant different ($p = 4 \times 10^{-7}$). Thus, with greatest mechanical stiffness perpendicular to the mean fiber direction. In the case of out-of-plane shear tests, the tests show average shear rupture stresses of $\overline{\tau}_{z\theta}^{u} = 750 \pm 239$ *kPa (mean $\pm$ SD)* in the circumferential and $\overline{\tau}_{\theta z}^{u} = 1272 \pm 473$ *kPa (mean $\pm$ SD)* in the longitudinal direction during shearing in the $z\theta$- and θz-modes. The mean values are significant different ($p = 0.0004$).

However, a remarkable feature has been found. There is a significant difference between in-plane and out-of-plane shear behavior of the material. The aortic media shows an order of magnitudes higher ultimate shear stress values for out-of-plane shear ($r\theta$-plane and rz-plane) than for in-plane shear ($z\theta$-plane). It follows that the material behaves much weaker at shearing in the in-plane direction than in the out-of-plane direction. Thus, one can assume that under mixed shear loading state, the tissue is going to fail due to low in-plane shear strength instead of out-of-plane shear strength.

For simple shearing of thoracic aortic tissue until the failure point in the different planes, it can be concluded that the strength increases in the following sequence: circumferential $<$ axial. In this context, several conclusions can be made. For example, to understand how a crack in the arterial wall propagates during aortic dissection, and furthermore, which stresses are necessary to induce this. During physiological loading state, very low shear forces due to blood flow act on the vascular wall.

Testing errors and limitations

Since no comparable data is available concerning the mechanical behavior during shearing up to failure of the tissue a high number of tests were performed to strengthen the meaningfulness of the results. Furthermore, statistical errors could be minimized and the validity of the results might be increased. The most common error causing testing abortion was due to the testing equipment. An extremely discouraging error sometimes occurred during testing, when the lower platform of the testing device moved relative to the fixed upper platform in the x-direction:

(i) *testXpert_Fehler Nr. 23402; Regelabweichung in Regler Transverse WN: 191977 ist zu groß*

Whenever either the upper or the lower side of the specimen detached from the fixed metallic stamps of the testing device during testing, the test was stopped and the collected data was removed to prevent any bias in the data evaluation. Note that at the beginning of developing the testing setup for this type of tissue shearing approximately every third test for in-plane shearing and every sixth test for out-of-plane shearing was successful. As already mentioned in Sec. 2.7.3 the use of sandpaper led to better attachment of the sample to the specimen holder and the rate of successful tests were significantly increased.

To further increase the efficiency concerning out-of-plane shear tests, different preparation procedures with sandpaper were tried. Two of these preparation geometries are shown in panel (a) and (b) of Fig. 4.1. However the tests of the small specimen still failed, mostly because of slipping out from the bottom side of specimen fixation. Subsequently, longer specimens were prepared to increase the adhesive surface for better attachment. Also the incision was introduced closer to the edge of the specimen as can be considered in panel (c) of Fig. 4.1. The antisymmetric double sided incision led to an improved situation of crack propagation.

As previously stated, the data after reaching the maximum stress point, where the propagation of the crack began with an angle, are not utilizable. However, it is worth mentioning

that there were two cases of crack propagation observed. On the one hand, it was the case that the crack spread parallel to the shear surface and on the other hand the crack propagated at first parallel to the sheared surface and then with an angle to the longer edge. An example for crack propagation can be seen in panel (d) of Fig. 4.1.
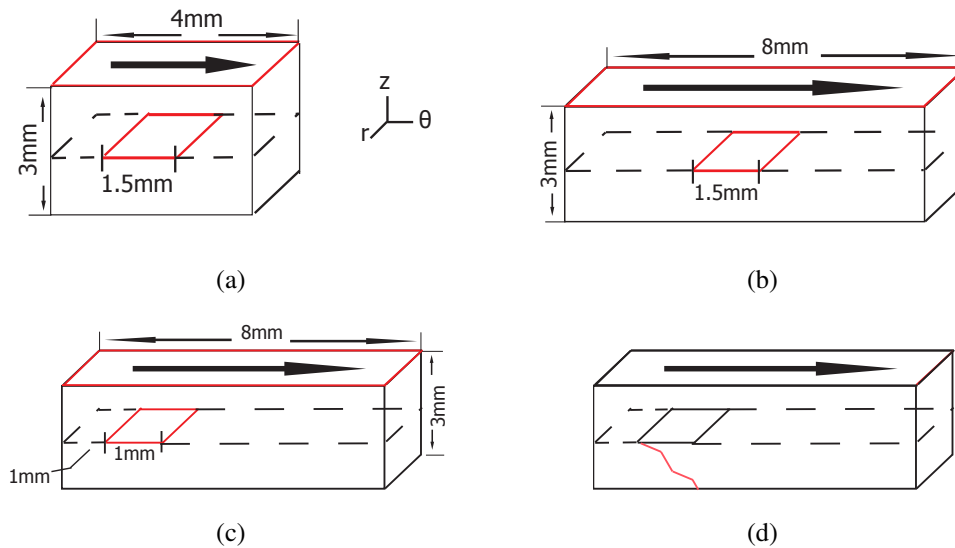
Figure 4.1: Sketches of the out-of-plane shear test specimens: (a) small size and (b) large size specimens, both having symmetrical double sided incisions. Panel (c) shows the final specimen preparation used for out-of-plane shear tests, with an anti-symmetrical incision, a dimension of 8mm $\times$ 3mm, and a length of 1mm of the sheared surface. In panel (d) crack propagation is shown.

4.5 Comparison of mechanical behavior due to pathological aspects

It is important to bear in mind that the non-athereosclerotic intimal thickening increases with age, where collagen fibers are deposited in the intimal layer (Movat et al., 1958). There were correlations between the anamnesis of a patients, see Table 2.1 in Sec. 2.1 and the mechanical properties of the tested arteries. The results of all conducted tests yield nearly the same behavior within the respective tests. Nevertheless, the absolute measured values vary within the individual samples.

Fluctuations in magnitudes within the different conducted tests may arise from donor properties and pathological aspects. As aforementioned in Sec. 1, aortic diseases affect mainly men. This trend is also confirmed by the number of male samples (10) vs. female samples (3) in this study.

Differences according to the age of the donor can be seen by a comparison of aneurysmatic specimens of donor *IX* (female, 58 yr) and *XII* (female, 72 yr). The younger donor, *IX*, exhibited stiffer results over all conducted tests that those of the older donor *XII*, which indicates tissue softening with age..

It is of high interest to see how the ultimate stresses differ with respect to the underlying tissue diseases (dissection, aneurysm, and so forth). Samples from dissected specimens *I*, *II*, *IV* and *XI* exhibit weaker response over all conducted tests than those of aneurysmatic specimens. It is therefore clear that the tissue composition of already dissected samples is not as strong as those of not dissected aneurysmatic samples.

Donor samples of specimen *III*, *VII* and *X* have, besides their aneurismatic causes, Marfan syndrome and Mass syndrome. They show on average the lowest ultimate strength values of all conducted tests. This reflects the high risk of patients with Marfan- or Mass syndrome to suffer an aortic dissection.

Very interesting facts can be seen for donor sample *III*. The reception of two different tissue samples *III*b from the healthy section and *III*a from the aneurysmatic section of the thoracic aorta, allow a comparison of their tissue properties. Due to the specimen size it was not possible to obtain all data of sample *III*a and *III*b, nonetheless from the conducted direct tension tests and in-plane shear tests one can see that the healthy section of sample *III*b is stronger than the tissue of the diseases section of sample *III*a.

Nonetheless, the relatively small amount of tested samples (13 thoracic aortas) may contribute to inadequate statistically relevant results. In the future more experimental tests should be conducted to receive more experimental data of more samples to validate the results presented in this work.

4.6 Conclusion

In summary, thirteen human thoracic aortic tissues have been investigated. The main conclusions are that the aortic media increases its strength under tension loading as follows: radial (normal direction) < axial (cross-fiber direction) < circumferential (fiber direction). Furthermore, this thesis shows new consolidated findings that the media is much stronger (almost an order of magnitude) under out-of-plane shear loading than under in-plane shear loading. The results show clearly interspecimen differences because of the anamnesis of the donors, such as age, diseases, and other risk factors. Anisotropic as well as nonlinear tissue properties are apparent from all experimental data.

The combination of uniaxial tension tests and simple shear testing data build a good information basis for modeling tissue mechanics. The obtained data are intended to be used for developing of a 3D failure criterion for the healthy and dissected human aortic media.

Bibliography

I. Akin, S. Kische, T. Rehders, H. Ince, and C. Nienaber. Acute aortic syndromes. *Medicin*, 38:450–455, 2010.

B. Alberts, A. Johnson, J. Lewis, M. Raff, K. Roberts, and P. Walter. *Molecular Biology of the Cell*. Garland Science, New York, 4th edition, 2007.

M. Arslan-Kirchner, Y. v. Kodolitsch, and J. Schmidtke. Genetische diagnostik beim marfan-syndrom und verwandten erkrankungen. *Deutsches Ärzteblatt*, Juli 2008.

I. A. L. Ayala and Y. F. Chen. Acute aortic dissection: An update. *Kaohsi*, 28:399–305, 2012.

A. Badrek-Amoudi, C. K. Patel, T. P. C. Kane, and S. E. Greenwald. The effect of age on residual strain in the rat aorta. *Journal of Biomedical Engineering*, 118:440–444, 1996.

G. V. R. Born and P. D. Richardson. Mechanical properties of human atherosclerotic lesions. In S. Glagov, W. P. Newman, and S. A. Schaffer, editors, *Pathology of Human Atherosclerotic Plaques*. Springer-Verlag, New York, 1990.

A. C. Burton. Relation of structure to function of the tissues of the wall of blood vessels. *Physiological Reviews*, 34:619–642, 1954.

S. S. Chen, N. T. Wright, and J. D. Humphrey. Heat-induced changes in the mechanics of a colcollagen tissue: isothermal, isotonic shrinkage. *ASME Journal of Biomechanical*, 117:86–93, 1998.

F. J. Criado. Aortic dissection. *Texas Heart Institute Journal*, 38:694–700, 2011.

H. Demiray and R. P. Vito. A layered cylindrical shell model for an aorta. *International Journal of Engineering Science*, 29:47–54, 1991.

M. Dietel, N. Suttorp, and M. Zeitz. *Harrisons Innere Medizin: Deutsche Ausgabe. In Zusammenarbeit mit der Carite*. ABW Wissenschaftsverlag GmbH, 2005.

S. Dokos, B. H. Smaill, A. A. Young, and I. J. LeGrice. Shear properties of passive ventricular myocardium. *Am J Physiol Hearth Circ Physiol*, 283:H2650–H2659, 2002.

R. Franken, A.W. Hartog, V. Waard, L. Engele, and T. Radocin. Circulating transforming growth factor-ß as a prognostic biomarker in marfan syndrome. *International Journal of Cardiology*, 168:2441–2446, 2013.

Y. C. Fung, K. Fronek, and P. Patitucci. Pseudoelasticity of arteries and the choice of its mathematical expression. *Am J Physiol Hearth Circ Physiol*, 237:H620–H631, 1979.

J. Golledge and K. A. Eagle. Acute aortic dissection. *Lancet*, 372:55–66, 2008.

G. N. Greaves, A. L. Greer, and R.S. Lakes. Poisson's ration and modern materials. *Nature Materials*, 10:823–837, 2011.

P. G. Hagan, C. A. Nienaber, E. M. Isselbacher, and D. Bruckman. The international resgistry of acute aortic dissection (irad): new insights into an old disease. *American Medical Association*, 283:897–903, 2000.

H. C. Han and Y. C. Fung. Residual strains in porcine and canine tracheas. *Journal of Biomechanics*, 24:307–315, 1991.

G. Herold. *Innere Medizin*. G. Herold, 2013.

R. B. Hickler. Aortic and large artery stiffness: Current methodology and clinical correlations. *Clinical Cardiology*, 13:317–322, 1990.

G. A. Holzapfel, T. C. Gasser, and R. W. Ogden. A new constitutive framework for arterial wall mechanics and a comparative study of material models. *Journal of Elasticity*, 61: 1–48, 2000a.

G. A. Holzapfel, C. A. J. Schulze-Bauer, and M. Stadler. Mechanics of angioplasty: Wall, balloon and stent. In J. Casey and G. Bao, editors, *Mechanics in Biology*, New York, 2000b. The American Society of Mechanical Engineers (ASME). AMD-Vol. 242/BED-Vol. 46, pp. 141–156.

G. A. Holzapfel, G. Sommer, and P. Regitnig. Anisotropic mechanical properties of tissue components in human atherosclerotic plaques. *Journal of Biomechanical Engineering*, 126:657–665, 2004.

G. A. Holzapfel, G. Sommer, and C. T. Gasser. Determination of layer-specific mechanical properties of human coronary arteries with nonatherosclerotic intimal thickening and related constitutive modeling. *Am J Physiol Hearth Circ Physiol*, 289:2048–2058, 2005.

G. A. Holzapfel, G. Sommer, M. Auer, P. Regitnig, and R. W. Ogden. Layer-specific 3D residual deformations of human aortas with non-atherosclerotic intimal thickening. *Annals of Biomedical Engineering*, 35:530–545, 2007.

J. Hulthe and B. Fagerberg. Circulating oxidized LDL is associated with subclinical atherosclerosis development and inflammatory cytokines (AIR study). *Arterioscler Thromb Vasc Biol.*, 22:1162–1167, 2002.

J. D. Humphrey. *Cardiovascular Solid Mechanics. Cells, Tissues, and Organs*. Springer-Verlag, New York, 2002.

IRAD, 2014. URL `http://www.iradonline.org/irad.html`. Access at 27.01.2015.

D. P. Judge and H. C. Dietz. Marfas's syndrome. *Lancet*, 2005.

T. Kang, J. Resar, and J.D. Humphrey. Heat-induced changes in the mechanical behavior of passive coronary arteries. *J Biomech Eng*, 117:86–93, 1995.

Michael Kutschera. Shear properties of passive ventricular porcine and human myocardium. Master's thesis, Graz University of Technology, 2012.

R. W. Lawton. The thermoelastic behavior of isolated aortic strips of the dog. *Circulation R*, pages 344–353, 1954.

G. L. Lendon, M. J. Davies, P. D. Richardson, and G. V. R. Born. Testing of small connective tissue specimens for the determination of the mechanical behaviour of atherosclerotic plaques. *Journal of Biomechanical Engineering*, 15:27–33, 1993.

H. M. Loree, A. J. Grodzinsky, S. Y. Park, L. J. Gibson, and R. T. Lee. Static circumferential tangential modulus of human atherosclerotic tissue. *J Biomech*, 27:195–204, 1994.

A. J. Lusis. Atheroslerosis. *National Institute of Health*, 407:233–241, 2000.

N. F. MacLean, N. L. Dudek, and M. R. Roach. The role of radial elastic properties in the development of aortic dissections. *Journal of Vascular Surgery*, 29:703–710, 1999.

D. Mohan and J. W. Melvin. Failure properties of passive human aortic tissue. I – uniaxial tension tests. *Journal of Biomechanics*, 15:887–902, 1982.

Ingrid Moll. *Dermatologie*. Number 458 - 459. Thiem, Germany, 6th edition, 1989.

U. Moog and O. Rie. *Medizinische Genetik für die Praxis*. Thiem, 2014.

H. Z. Movat, R. H. More, and M. D. Haust. The diffuse intimal thickening of the human aorta with aging. *American Journal of Pathology*, 34:1023–1031, 1958.

W. W. Nichols and M. F. O'Rourke. *McDonald's Blood Flow in Arteries. Theoretical, Experimental and Clinical Principles*. Arnold, London, 4th edition, 1998.

P. J. Oberwalder. Aneurysmen und dissektionen der thorakalen aorten: Definition und pathologie. *Austrian Journal of Cardiology*, 8:2–4, 2001a.

P. J. Oberwalder. Die chirurgie der aorta ascendens und des aortenbogens bei aneurysmen und dissektionen. *Austrian Journal of Cardiology*, 8:19–24, 2001b.

J. W. Olin and V. Fuster. Acute aortic dissection. *American Heart Association*, 23:1721–1723, 2003.

D. J. Patel and D. L. Fry. The elastic symmetry of arterial segments in dogs. *Circulation Research*, 24:1–8, 1969.

H. R. Polster, S. Krautzig, and J. Braun. *Basislehrbuch Innere Medizin*. ELSEVIER, 2008.

J. A. G. Rhodin. Architecture of the vessel wall. In R. M. Berne, editor, *Handbook of Physiology, Section 2, Volume 2*. Am Physiol Soc, Bethesda, 1979.

A. J. Schriefl, G. Zeindlinger, D. M. Pierce, P. Regitnig, and G. A. Holzapfel. Determination of the layer-specific distributed collagen fiber orientations in human thoracic and abdominal aortas and common iliac arteries. *Journal of the Royal Society*, 9:1275–1286, 2012.

G. H. Sodeck, M. Czerny, and H. Domanovits. Akute thorakale aortendissektion - altbekanntes und neues. *J Kardiol*, 5:15–19, 2008.

G. Sommer. *Mechanical Properties of Healthy and Diseased Human Arteries*. Technische Universität Graz, 2010.

G. Sommer, T. C. Gasser, P. Regitnig, M. Auer, and G. A. Holzapfel. Dissection properties of the human aortic media: an experimental study. *Journal of Biomedical Engineering*, 130:021007–1–12, 2008.

G. Sommer, A. Schriefl, G. Zeindlinger, A. Katzensteiner, H. Ainödhofer, A. Saxena, and G. A. Holzapfel. Multiaxial mechanical response and constitutive modeling of esophageal tissues: impact on esophageal tissue engineering. *Acta Biomaterialia*, 9: 9379–9091, 2013.

M. Thalmann, G. H. Sodeck, H. Domanovits, and M. Grassberger. Acute type a aortic dissection and pregnancy: a population-based study. *European Journal of Cardio-Thoracic Surgery*, 39:159–163, 2011.

J. Tong, G. Sommer, P. Regitnig, and G. A. Holzapfel. Dissection properties and mechanical strength of tissue components in human carotid bifurcations. *Annals of Biomedical Engineering*, 39:1703–1719, 2011.

L. D. T. Topoleski, N. V. Salunke, J. D. Humphrey, and W. J. Mergner. Composition- and history-dependent radial compressive behavior of human atherosclerotic plaque. *Journal of Biomedical Materials Research*, 35:117–127, 1997.

R. P. Vito and H. Demiray. A two layered model for arterial wall mechanics. In *Proceedings of the 35th Annual Conference on Engineering in Medicine and Biology (ACEMB)*, Pennsylvania, PA, 1982. September 22–24, 1982.

H. Weisbecker, D. M. Pierce, P. Regitnig, and G. A. Holzapfel. Layer-specific damage experiments and modeling of human thoracic and abdominal aortas with non-atherosclerotic intimal thickening. *Journal of the Mechanical Behavior of Biomedical Materials*, 12:93–106, 2012.

D. Wen, X. L. Zhou, J. J. Li, and R. T. Hui. Biomarkers in aortic dissection. *Clinica Chimica*, 9:688–695, 2011.

D. Wu, Y. H. Shen, L. Russell, J S. Coselli, and S. A. LeMaire. Molecular mechanisms of thoracic aortic dissection. *Journal of Surgical Research*, 29:907–924, 2013.

X. Zhang, Y. H. Shen, and S. A. LeMaire. Thoracic aortic dissection: Are matrix metalloproteinases involved? *Vascular*, 17:147–157, 2009.

Statutory Declaration

I declare that I have authored this Thesis independently, that I have not used other than the declared sources/resources, and that I have explicitly marked all material, which has been quoted by the relevant reference.

_____
date

_____
signature